12-2016

Low temperature flexible perovskite solar cell with mesoporous TiO2 electron transport layer in high humidity environment

Felipe De La Torre
The University of Texas Rio Grande Valley

LOW TEMPERATURE FLEXIBLE PEROVSKITE SOLAR CELL WITH MESOPOROUS TiO_2 ELECTRON TRANSPORT LAYER IN HIGH HUMIDITY ENVIRONMENT

A Thesis

by

FELIPE DE LA TORRE

Submitted to the Graduate College of
The University of Texas Rio Grande Valley
In partial fulfillment of the requirements for the degree of

MASTER OF SCIENCE ENGINEERING

December 2016

Major Subject: Electrical Engineering

LOW TEMPERATURE FLEXIBLE PEROVSKITE SOLAR CELL WITH MESOPOROUS TiO_2 ELECTRON TRANSPORT LAYER IN HIGH HUMIDITY ENVIRONMENT

A Thesis
by
FELIPE DE LA TORRE

COMMITTEE MEMBERS

Dr. Karen Lozano
Co-Chair of Committee

Dr. Jaime Ramos
Co-Chair of Committee

Dr. Horacio Vasquez
Committee Member

Dr. Heinrich Foltz
Committee Member

December 2016

ABSTRACT

De La Torre, Felipe, Low Temperature Flexible Perovskite Solar Cell with Mesoporous TiO_2 Electron Transport Layer in High Humidity Environment. Master of Science Engineering (MSE), December, 2016, 76 pp., 8 tables, 31 figures, references, 81 titles.

Perovskite solar cells are the fastest advancing solar technology to date with efficiencies increasing from 3.9% to more than 21% within a few years. They have emerged as a possible alternative to silicon photovoltaics due to their exceptional photovoltaic performance, light absorbing properties, and low-cost fabrication with methylammonium lead iodide ($CH_3NH_3PbI_3$) getting considerable interest in research and development. However, there are still many challenges that must be addressed for perovskite solar cells to replace contemporary solar cells, such as improving their stability, making them nonhazardous, further increasing their efficiency, and developing better techniques for large scale fabrication. In this thesis, a low temperature flexible perovskite solar cell that uses a mesoporous TiO_2 layer as the electron transport layer was developed capable of producing efficiencies up to 4.82% for active areas of $0.01cm^2$ and 1.84% for active areas of $0.12cm^2$.

DEDICATION

To my amazing wife

Dulce De La Torre

To my parents

Mr. and Mrs. Felipe and Patricia

De La Torre

and

To my siblings

Luis and Brenda

This work would not have been

Possible without you.

ACKNOWLEDGMENTS

There are many people that I would like to thank for helping me while I was working on my research. First, I would like to thank Dr. Karen Lozano for encouraging and supporting me to work on my thesis. For all of her guidance, encouragement, and patience. I would also like to thank Dr. Ramos, Dr. Vasquez, and Dr. Foltz for serving on my committee and taking time to assist me when I needed it. Special thanks to Omar Torres for making me push myself and for helping me in during the difficult times when it felt like I wasn't going to be able to succeed. Hilario Cortez, your help with the SEM and the lab equipment was essential in order for me to be able to finish my work and Ms. Lisa thank you for all of your assistance throughout the time that I was working with Dr. Lozano. I would also like to thank my fellow PREM students for all of their support.

This project is supported by NSF PREM award under grant No. DMR-1523577: UTRGV-UMN Partnership for Fostering Innovation by Bridging Excellence in Research and Student Success.

TABLE OF CONTENTS

Page

LIST OF TABLES

Page

LIST OF FIGURES

CHAPTER I

INTRODUCTION

1.1 Thesis Introduction

1.1.1 Statement of Problem

Currently the majority of research conducted for perovskite solar cells that use TiO_2 as the electron transport layer have a compact TiO_2 layer which requires a rigid glass substrate in order to use high temperatures that reach up to 500°C. These solar cells have been able to produce high efficiencies but are limited with the locations that they could be used for because a flat surface would be needed to prevent them from breaking.

1.1.2 Statement of Purpose

The inspiration of this project was to fabricate a low cost flexible perovskite solar cell that could be fabricated in air environment. In order to be able to fabricate flexible perovskite solar cells while maintaining a low fabrication cost, a plastic substrate is needed which requires low temperature to prevent it from undergoing from thermal stress which would cause it to deform. Typically PEDOT:PSS has been used as the electron transport layer due to its low temperature annealing requirement but it has a higher cost than TiO_2. In order to fabricate an inexpensive flexible perovskite solar cell, a mesoporous TiO_2 film is needed for the electron transport layer. Poly (3-hexylthiophene-2,5-diyl), P3HT, is also a great substitute to the popular hole transport

material Spiro-OMeTAD due to its lower price and capability to produce solar cells with high efficiencies.

There are five chapters in this thesis.

In chapter 2, a general introduction to perovskite solar cells is given with some of the most popular techniques that are currently used to fabricate them along with a brief introduction on different types of solar cells such as those that include nanofibers, dye sensitized solar cells, and solid state perovskite solar cells. A more in depth discussion is given for current perovskite solar cell research that has been made in air environment, the effects that the thickness and morphology of the layers have on the efficiency of the cells, techniques used for large scale fabrication, low temperature fabrication techniques, the effects on the stability of the cells, simple structures that are used, and other methods that are used to increase the efficiency.

In chapter 3, the experimental setup is discussed showing the different equipment that was needed for the fabrication and characterization of the perovskite solar cells with a description of what each of the systems does on the fabrication process. Chapter 4 covers the experimental procedure which includes the materials that were needed along with the procedure to make the solutions needed to fabricate the perovskite solar cells, the steps needed for the fabrication of the cells, and an explanation on the characterization parameters needed to calculate how the cells are performing.

In chapter 5, the layer characterization of the cells are discussed with an explanation on how different fabrication parameters were affecting the perovskite solar cell's performance and layer morphology. Lastly, chapter 6 concludes the thesis along with future work that could help further improve the perovskite solar cells.

CHAPTER II

REVIEW OF LITERATURE

2.1 Introduction

Today's society relies heavily on electricity to power a great variety of electronics, appliances, and residential electrical devices. In 2015, the average annual electricity consumption for a U.S. residential utility customer was 10,812 kWh ("How much electricity", 2016) which keeps increasing as electricity becomes a greater necessity for all types of new residential technologies and gadgets that need to be powered. With a limited supply of fossil fuels to keep up with mankind's demands in the long term, finding a sustainable energy source is currently a major challenge. Renewable energy sources (biofuels, biomass, geothermal, hydropower, solar, and wind) have the potential to replace fossil fuels and supply clean and sustainable energy. During a sunny day, an area the size of a small backyard (48 m^2) can receive about 288 kWh which is approximately 10 times what the average U.S. household daily usage ("Energy from the sun", 2015). This is the reason why solar energy is a promising candidate for supplying residences with the energy demand.

The present dominant photovoltaic (PV) technology is silicon-based with high material and manufacturing costs limiting its widespread production. Research has been conducted towards developing low cost PV technologies of which perovskite solar cells (PSC) are a promising option (Li, N., 2016). An efficient solar cell must be able to absorb a wide electromagnetic wavelength

range from visible to near infrared wavelengths (350 to ~950 nm) and be able to convert the light energy effectively into electricity. This electricity must be collected at high voltages and currents in order to be useful (Lee, M. et al., 2012), which could be achieved with perovskite solar cells.

2.1.1 Background of Perovskite Solar Cells

Perovskite materials have a crystal structure **(Figure 2.1)** with the basic ABX_3 formula (X = oxygen, halogen). The larger cation "A" occupies a cubo-octahedral site shared with twelve "X" anions while the smaller cations "B" stabilize in the octahedral site shared with six "X" anions (N.G. Park, 2015). The general principle of a PSC consists of photons exciting the atoms in the active layer which causes the electrons and holes to travel towards the electron and hole transport layer contacts. Then, electricity flows towards the electrical load being powered.

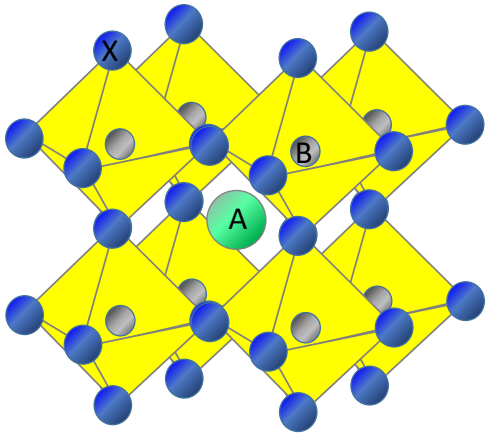

Figure 2.1: Perovskite Crystal Structure

In PSCs, the active absorber layer is placed between the electron and hole transport layers (ETLs and HTLs, respectively) (Cao, K., 2015). Common ETLs and HTLs are usually composed of TiO_2 and 2,2',7,7'-tetrakis-(N,N-di-p-methoxyphenylamine)-9, 9'-spiro-bifluorene (spiro-MeOTAD), respectively (Q. Chen, 2014). Modern PSCs include spiro-OMeTAD as a hole-

transport material (HTM) in combination with inorganic interlayers allowing for an efficient charge transport system. In order to further reduce the fabrication cost of PSCs, removal or replacement of this expensive HTM layer is required without affecting the stability of the device. Methylammonium lead halide perovskites ($MAPbX_3$) are regarded as promising light absorbers due to their advantages with high absorption coefficients, large electron-hole diffusion length, and optical band gaps (Stoumpos, C. et al., 2013; Liu, D. et al., 2014; Miller, D. et al., 2012; Choi, H. et al., 2014) allowing them to be used in thin-film solar cells with a planar heterojunction (PHJ) structure (Liu, D. et al., 2014; Malinkiewicz, O., 2014). Moreover, they exhibit ambipolar transport properties which are capable of transporting both holes and electrons simultaneously (Chung, I. et al., 2012; Etgar, L. et al., 2012). These properties have provoked development of new device structures for efficient energy conversion (Kazim, S. et al., 2014). Furthermore, uniformity of the perovskite layer and the efficiency of extracting free charge carriers through the ETLs and HTLs are important factors to be optimized in order to increase the power conversion efficiencies (PCE) (Heo, J. H. et al., 2014; You, J. et al., 2014, Guo, Y. et al., 2014).

Significant breakthroughs have been achieved in perovskite solar cells with power conversion efficiencies (PCE) increasing from 3.8% to over 22.1% within 6 years making this technology comparable to crystalline silicon and thin film technologies (Liu, D. and Kelly, T., 2014; Park, G., 2015). Miyasaka et al. (Kojima, A. et al., 2009) demonstrated efficiencies of 3.1% and 3.8% for X being Bromine and Iodine, respectively. Snaith *et al.* reported a solution-processed P-PSC with a p-i-n heterojunction structure (Ball, J.M., et al., 2013) where the perovskite film is layered between the p-type material such as PEDOT:PSS or spiro-MeOTAD and the n-type material such as compact TiO_2 or PCBM (Xing, G.C. et al., 2013; Zhou, H.P. et al., 2014). Perovskite materials can have compatibility issues between the photo absorber and the cell's

structure being used. A comparison between $CH_3NH_3PbI_3$ and $CH_3NH_3PbI_{3-x}Cl_x$ in a planar and mesoporous structure (Shi, Y., et al., 2015) demonstrate that the light absorption, crystallinity, surface coverage, and dissociation of photo-generated electrons of the perovskite can be considerably different. Mesoporous and planar devices produced efficiencies of 14.05% and 6.76%, respectively, when $CH_3NH_3PbI_3$ was used. In comparison, $CH_3NH_3PbI_{3-x}Cl_x$ produced efficiencies up to 12.67% and 7.87% in planar and mesoporous devices, respectively.

It is currently a challenge to control thin-film morphology of perovskite layers which has shown that poor film morphology results in low shunt resistance and less light absorption; impacting the photoelectric conversion process (Eperon, G.E., et al., 2014; Jeng, J. Y. et al, 2013). The process to deposit the perovskite layer greatly impacts the device's performance. It can affect the film's morphology due to the presence of pinholes and imperfections which leads to a decrease of open circuit voltage (V_{OC}) and short circuit current density (J_{SC}). The perovskite deposition procedures consist of the one step and two step solution deposition, with the most common and simplest method being the one step due to the direct deposition of perovskite precursor solution on top of mesoscopic or planar oxide. Unfortunately, it is difficult to make high quality continuous perovskite films by spin coating lead iodide (PbI_2) and methylammonium halide (CH_3NH_3I) due to rapid crystallization of $CH_3NH_3PbI_3$ (Chen, Q. et al., 2014). To achieve reproducible perovskite film morphology, a two-step deposition technique has been developed which consists of applying a PbI_2 based solution onto the ETL (Wu, Y. et al., 2014) or mesoporous scaffold (Bi, D. et al., 2013) followed by dip coating the substrate into the methylammonium iodide solution in isopropanol (IPA). Ma et al. (Ma, Y. et al., 2014) and Im et al. (Zhang, W. et al., 2015) have reported an improved morphology of the perovskite films in comparison to the single step procedure making them more uniform and reproducible. Another method consists of depositing

the PbI_2 by spin coating as it is exposed to CH_3NH_3I vapor in N_2 atmosphere to create the perovskite layer. This method allows for good surface coverage, low surface roughness and excellent film quality with efficiencies of 12.1% (Chen, Q. et al., 2013). It is also possible to produce the perovskite layer using vapor deposition techniques, where the perovskite growth is achieved without the need of using any solvent. There are several different vapor deposition techniques that have demonstrated an improved film uniformity and surface coverage of the active layer (Hu, H. et al., 2014). Unfortunately, those techniques do not allow for easy fabrication as the source temperature must be closely controlled due to the relatively low thermal stability of the perovskite precursors.

Current commercialized silicon-based solar cells guarantee a 25-year lifetime. A critical issue that must be addressed is the long term stability of the PSC in order to be able to compete against their silicon counterpart. Many factors are at fault for the degradation of perovskite materials which include: oxygen and moisture (Niu, G. et al., 2013; Liang, Y. Y. et al., 2010) migration of electrode metal through the hole-transfer materials to interact with the perovskite film (Guarnera, S. et al., 2015), decay of perovskite material due to UV light exposure (Leijtens, T. et al., 2013) and high temperatures (Dualeh, A. et al., 2014). High levels of humidity tend to affect perovskite solar cells; there is a study that produced a highly efficient solar cell (19.3%) when less than 30% humidity was present during the fabrication process (Zhou, H. et al., 2014).

2.2 Methods of Fabrication of Perovskites Solar Cells

The thickness of the layers of a solar cell can be critical in determining whether it will have a high open circuit voltage, short circuit current, fill factor, efficiency, and stability. There are

many different methods to achieve this. A range of techniques have been developed for the fabrication of perovskite solar cells, the most common being blade, spray, dip, and spin coatings.

2.2.1 Blade Coating

Blade coating, also known as knife coating or doctor blade coating, is a method used for the fabrication of large area films on rigid or flexible substrates. The thickness can be controlled by changing the distance between the blade and the substrate. For small scale fabrication, it can easily be achieved by applying an excess amount of the solution that needs to be applied to the substrate and manually sliding a blade across the substrate until the desired area is fully covered with the solution **(Figure 2.2)**.

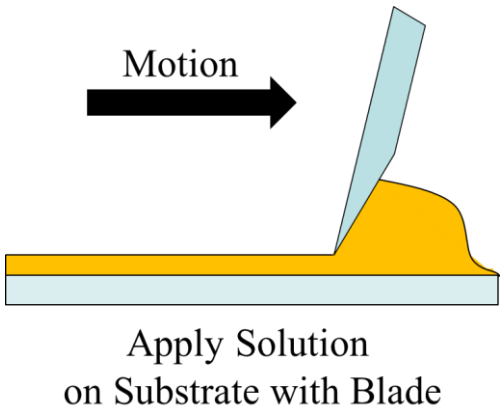

Figure 2.2: Blade Coating Technique

This method can also be used in large scale fabrication by applying the solution that needs to be spread behind the blade and having the substrate move towards the blade. The constant deposition of solution allows for a large amount of substrates to be continuously coated.

2.2.2 Spray Coating

Spray coating **(Figure 2.3)** consists of a solution being sprayed on a substrate. This allows for a continuous flow of droplets to adhere to the substrate which allow fast drying of the layers. Multiple layers can be applied in a short time due to the rapid evaporation of the solvent. This method allows a broad range of solvents to be used in creating the different layers of a solar cell. The film morphology can be controlled by the air pressure, solution viscosity, solvent properties, and the distance between the nozzle and substrate.

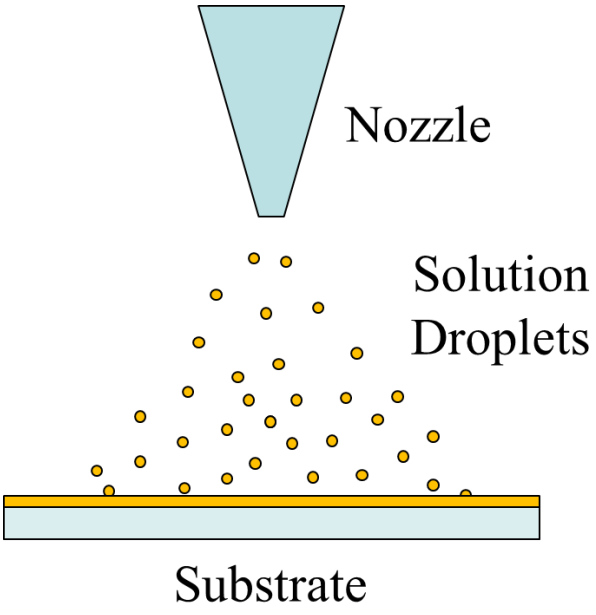

Figure 2.3: Spray Coating Method

2.2.3 Dip Coating

Dip coating **(Figure 2.4)** is the method used to apply nano-thick layers by immersing, or dipping, a substrate into the coating material at a constant speed. The substrate must stay on the solution for a while allowing the coating material to adhere to the substrate. It must then be slowly

removed from the solution, the speed in which it is pulled out determines the thickness that the layer will have. The slower that it is withdrawn, the thinner the layer will be. Excess solution must be removed from the substrate, this can be achieved by letting it drain or by dipping the substrate in water. To complete the process, the solvent must be evaporated thus forming a thin layer.

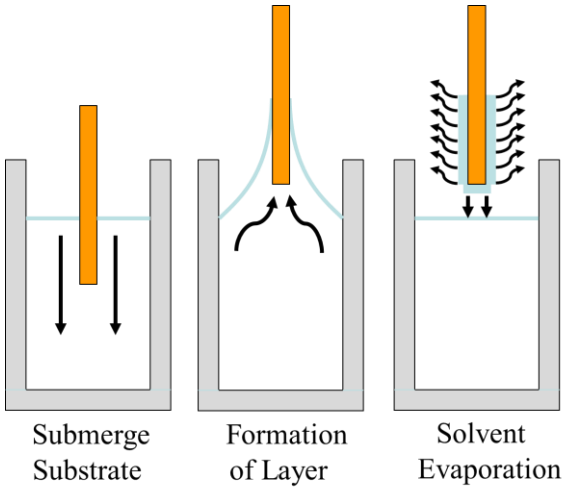

Figure 2.4: Stages for the dip coating method. Dipping substrate into solution, extracting substrate slowly to produce a thin layer, and allowing for the solvent to evaporate once the substrate is extracted

2.2.4 Spin Coating

Spin coating **(Figure 2.5)** is utilized to create thin layers by dispersing liquids uniformly on planar substrates. It consist of applying drops of solution on the substrate when stationary or while it is in slow motion and spinning it at high speeds for a short amount of time to spread the solution by centrifugal force. The faster and longer it spins, the thinner the layer will be. The solvent evaporates as the substrate is spinning. An advantage is being able to control the thickness of the layers by altering the time that the substrate is spinning, the speed, and the solution's

viscosity. The biggest disadvantages are the loss of excess coating materials and unavailability in larger scale fabrication.

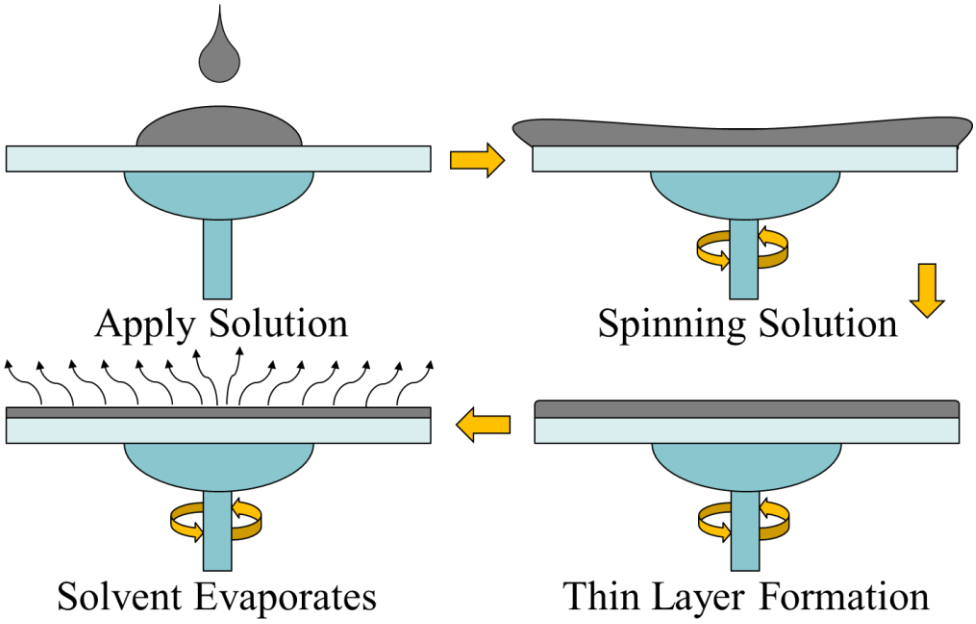

Figure 2.5: Liquid solution is applied to a substrate. The substrate is rotated slowly to disperse the solution. The speed is increased to give a desired thickness. Lastly, the substrate must remain rotating to evaporate the solvents.

2.2.5 One Step Deposition of Perovskite

The one step deposition **(Figure 2.6)** consists of applying $CH_3NH_3PbI_3$ onto the substrate then spin coating it in order to obtain a thin layer followed by annealing and the completion of the perovskite layer. This method is the most common due to its simplicity but has problems because of the rapid crystallization of $CH_3NH_3PbI_3$

2.2.6 Two Step Deposition of Perovskite

The two step deposition **(Figure 2.7)** consists of first applying a PbI_2 solution by spin coating followed by spin coating a CH_3NH_3I solution or dipping the substrate with the PbI_2 layer onto a CH_3NH_3I in isopropanol alcohol. The processes is then finished by annealing the substrate forming the perovskite layer. This method has been preferred over the one step deposition due to the improved morphology of the perovskite layer which has allowed for higher efficiencies to be obtained.

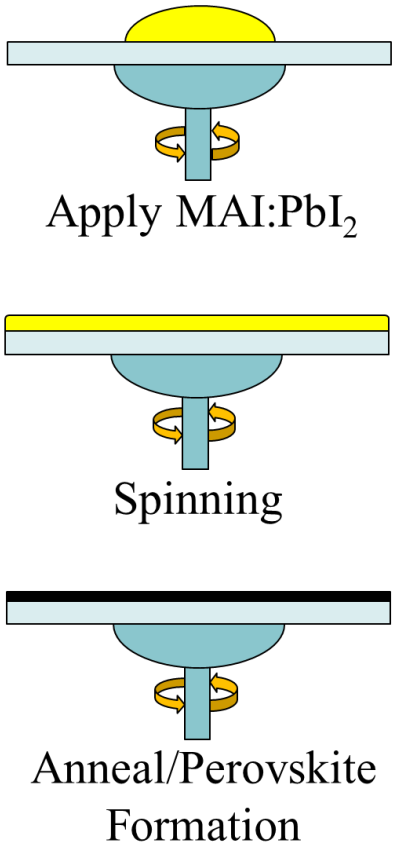

Figure 2.6: One Step Deposition of the Perovskite Layer

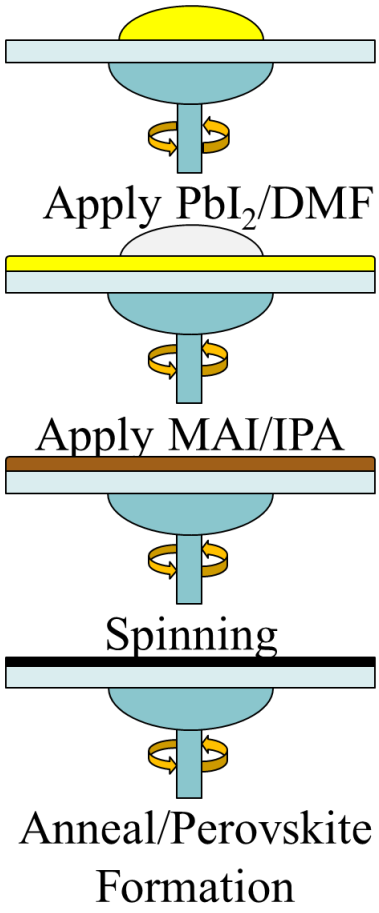

Figure 2.7: Two Step Deposition Method of the Perovskite Layer

2.3 Types of Solar Cells

2.3.1 Solar Cells with Nanofibers

Solar cells have been developed utilizing nanofibers in order to attempt to enhance their efficiency, stability, and low cost fabrication. Nanofibers have been shown to optimize morphologies directly upon deposition (Zhang, W. et al., 2015). Utilizing nanofibers allow traditional thermal treatment to become unnecessary allowing flexible substrates to be utilized (Ma, Y. et al., 2014). Nair, S. et al., 2011, developed a Pechini-type sol by electrospinning TiO_2 nanofibers with diameters ranging between 50 nm - 200 nm capable of producing a porous and

compact layer of TiO_2 upon doctor-blading and sintering. This method did not require adhesion and scattering of layers or $TiCl_4$ treatment. Under standard test conditions, they were able to produce a dye sensitized solar cell with an efficiency of ~4.2%.

The rate at which the TiO_2 solution is fed during electrospinning affects the diameter of the fibers and the efficiency of the solar cell. Mali, S. S. et al., 2015, experimented with different feeding rates of 1.0, 1.5, 2.0 and 2.5 ml h^{-1} in order to control the diameter of the TiO_2 nanofibers being produced. After applying a TiO_2 paste (synthesized from the produced nanofibers) with the blade-technique, the surface area of the TiO_2 nanofibers was measured at the N_2 adsorption-desorption isotherm by a Brunauer-Emmet-Teller (BET). It was found that the surface area was approximately two times greater when the feeding rate was at 1.5ml h^{-1} than at any other feeding rate. This high surface area is due to the formation of the TiO_2 nanofibers in a well interconnected network which allows for a greater amount of dye adsorption, fast electron transportation through interconnected network and effective light harvesting (Mali, S. S. et al., 2013). This resulted in an efficiency of 5.39%, which was 1.30% greater than those without nanofibers.

The nanofiber morphology also plays an important role on a cell's efficiency as discussed in (Bertho, S. et al., 2009) where they studied the effects of P3HT:PCBM nanofiber content per solution varying on temperatures ranging from 37 to 50°C. It was determined that the fiber content of the solutions decreases dramatically as the temperature is increased, from 60% to 14%. They were able to produce an optimal efficiency of ~3.2% for a solution with temperature of 45°C. **Figure 2.8** illustrates the change in fiber content, efficiency, short circuit current, open circuit voltage, and fill factor as temperature increases.

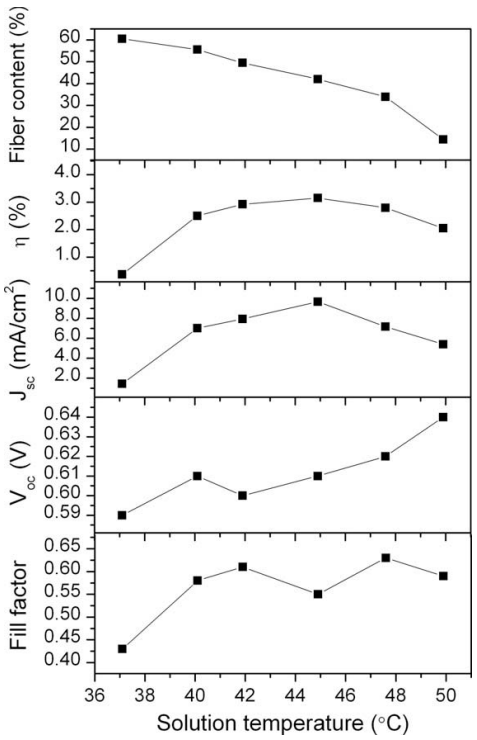

Figure 2.8: Fiber content of solutions, efficiency, short circuit current, open circuit voltage, and fill factor of nanofibers produced from P3HT:PCBM solar cells as a function of the solution temperature (S. Bertho et al., 2009)

Introducing quantum dots to the nanofibers enhance dye absorption in dye sensitized solar cells allowing higher efficiencies to be obtained. The authors in (Salam, Z. et al., 2015) introduced graphene quantum dots to electrospun TiO_2 nanofibers. It was observed that they improved the dye uptake enhancing the short circuit current and improving the stability of the dye sensitized solar cell. An efficiency of 4.81% was obtained from pure TiO_2 nanofibers and an efficiency of 6.22% after treating the TiO_2 nanofibers with the graphene quantum dots.

2.3.2 Dye Sensitized Solar Cells

Dye sensitized solar cells (DSSC) received considerable attention since 1991 due to their relative low fabrication cost and high power conversion efficiency (PCE) reaching 7% (Nagarjuna, P. et al., 2015) and have been under extensive research. Depending on the size and materials, their

efficiency varies between 5 - 10%. Most DSSCs consist of applying a TiO_2 layer and letting it absorb a dye. The dye is typically a metalorganic Ru-complex which is excited by absorption of a photon with the absorption range starting at 720 nm for most of the dyes. DSSCs have stability problems due to the use of liquid electrolyte. When utilized in a low temperature environment, the electrolyte can freeze which disrupts the power production. This can create some physical stress damaging the device. At higher temperatures, the electrolyte is capable of expanding which can cause it to spill if it's not properly sealed. Because of the chemically aggressive electrolyte, silver electrodes for current collection are not possible. This limits the size which they can be made since FTO becomes a limiting factor for cells greater than 1 cm^2 (Gratzel, M.). DSSCs tend to be costly due to the ruthenium dye, platinum, and conducting glass needed to fabricate them. The electrolyte is also hazardous to human health and the environment. In order to work around these issues, a new device was fabricated where the liquid electrolyte was replaced by a solid perovskite layer which acts as the hole conducting material allowing for cheaper fabrication of solar cells.

2.3.3 Solid-State Perovskite Solar Cells

PSCs are based on dye sensitized Gratzel solar cells. Gratzel developed a low cost photo-electrochemical solar cell based on high surface area nanocrystalline TiO_2 film sensitized with molecular dye (O'regan, B. and Gratzel, M., 1991). The properties of ABX_3 type perovskite materials are tunable by modifying 'A' (ammonium, lithium, silver, cesium, etc), 'B' (lead, tin, titanium, etc) and 'X' (fluride, iodide, bromide, chloride) or a combination of them. The most utilized perovskite in today's research is methyl ammonium lead iodide ($CH_3NH_3PbI_3$). This material dissolves in different solvents such as ϒ-butyrolactone (GBL), N,N-Dimethylformamide (DMF), N,N-dimethylacetamide (DMAc), or Dimethyl sulfoxide (DMSO) and it is deposited onto a mesoscopic TiO_2 film which is infiltrated with a hole transport material.

The basic working principle of a PSC **(Figure 2.9)** consists of the production of energy through excitons (electron-hole pairs). Photons hitting the active area, in this case being the perovskite material, cause for negatively charged electrons to become excited and move to a higher energy band. The holes, or positive charges, are created on the molecules where the electron becomes absent. An ETL and HTL are needed in order for the exciton to detach into an electron and hole to allow them travel to the anode and cathode respectively.

Figure 2.10 illustrates the basic structure of a solid-state perovskite solar cell. To prevent direct contact between the HTM and transparent conductive oxide, a compact TiO_2 layer is required as ETL. A compact ETL is essential to prevent the charge recombination originated in the FTO electrode and hole conducting layer allowing for higher efficiencies to be achieved (Deng, J. et al., 2014). The foundation of a solid-state cell is similar to that of a dye-sensitized solar cell but it has a solid HTM layer instead of the liquid electrolyte, which improves the device's stability compared to DSSCs.

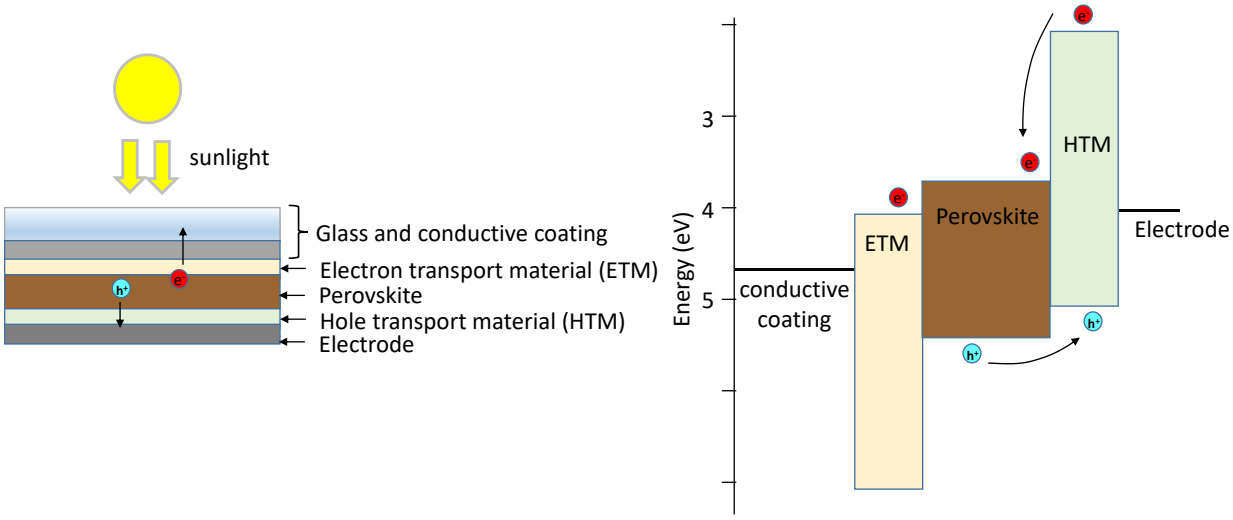

Figure 2.9: Working Principle of a Perovskite Solar Cell

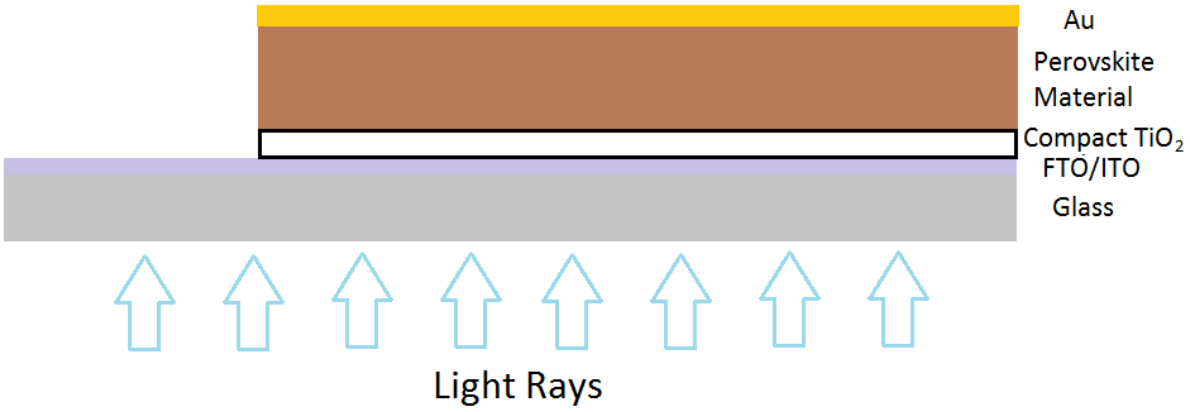

Figure 2.10: Basic Structure of a Perovskite Solar Cell

By utilizing perovskite sensitized materials it is possible to enable the reduction of the material bandgap and increase the open circuit voltage; an increase in the photovoltaic performance is possible by incorporating perovskite material into polymer absorbers. **Figure 2.11** summarizes the effects obtained by including a layer of $CH_3NH_3PbI_3$ between poly[(4,8-bis-(2-ethylhexyloxy)-benzo[1,2-b;4,5-b']dithiophene)-2,6-diyl-alt-(4-(2-ethylhexanoyl)-thieno[3,4-

b]thiophene)-2,6-diyl] (PBDTTT-C), polythieno[3,4-b] thiophene/benzodithiophene (PTB7) and poly[4,8-bis(5-(2-ethyl-hexyl)thiophen-2-yl)benzo[1,2-b:4,5-b']dithiophene-co-3-fluor-othieno[3,4-b]thiophene-2-carboxylate] (PTB7-Th) (Huang, L. et al., 2015). The addition of $CH_3NH_3PbI_3$ in the solar cells had significant increase in V_{OC} compared to their corresponding single junction solar cells, proving that incorporating perovskite materials in solar cells can improve the V_{OC} and overall photovoltaic performance.

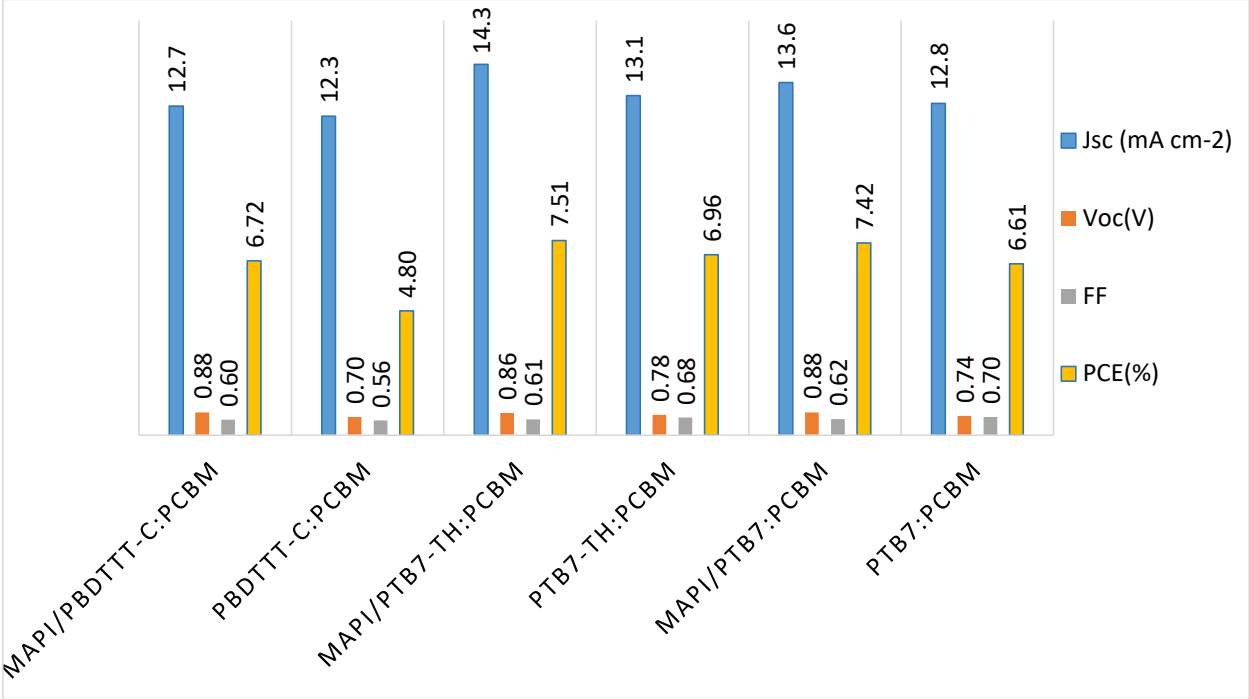

Figure 2.11: Comparison of photovoltaic performance between devices with perovskites and those without based on three polymers

2.3.3.1 Fabrication in Air Environment. A major issue when fabricating a PSC is that some processes must be done using a high vacuum or an inert atmosphere inside a glove box. Research has been done in ambient air environment in order to facilitate the fabrication process of PSC and further decrease their cost. Casaluci, S. et al., 2015, developed a cheap and quick double step vapor deposition technique based on vapor-assisted solution processing (V-VASP). The

preparation of the active layer was done in air with a low vacuum in order to prevent any moisture from being in the environment. The annealing time of PbI_2 in air using different solvents such as GBL, DMF, and DMSO was studied during the first stage. The growth time of the perovskite layer was optimized for both planar and mesoporous perovskite solar cells for the second stage as shown in **Table 2.1**. A top efficiency of 12.7% was achieved for a P-PSC and over 11% for a M-PSC with uniform film morphology. Using V-VASP showed improved stability even though methylammonium lead iodide is sensitive to oxygen and moisture. The perovskite films did not suffer any discoloration or crystalline lead iodide in the films after 14 days while stored in air at 20°C and 50% humidity without encapsulation.

Table 2.1: Photovoltaic Parameters of Deviceds in Air Environment (S. Casaluci et al., 2015)

Cell Parameters - devices with 10 pixels				Performance of best pixel			
Solvent	Perovskite growth time	Cell type	Average PCE [%]	V_{oc} [mV]	J_{sc} [mA cm^{-2}]	Fill factor [%]	Best PCE [%]
DMF	30 min	Planar	10.2	950	17.9	65.7	11.2
	1 hr		11	967	19.5	67.5	12.7
	2 hr		5.3	900	10.3	63.9	5.9
	1 hr	Mesoporous	9.1	920	17.2	63.5	10
	2 hr		3.3	830	11.3	60	5.6
DMSO	30 min	Planar	9	972	17.5	65.2	11
	1 hr		3.5	757	13.3	44	4.4
	2 hr		5.5	820	12.8	54	5.7
	3 hr		7.1	852	16.5	61.2	8.6

2.3.3.2 Thickness and Film Morphology. Presently, a major challenge for producing high efficiency PSCs has been the ability of controlling the film thickness and morphology of the perovskite layers (Hu, X. et al., 2015). Poor film morphology can result in low shunting resistance, less light absorption, and can impact the photoelectric conversion process (Liang, P. W. et al., 2014). It has been demonstrated that the uniform perovskite films as well as non-mesoporous layer can be achieved by controlled the solvent atmosphere and annealing temperature during the thin-film process (Eperon, G. E. et al., 2014). Crystallization of perovskite films can be enhanced by

integrating solvent-processing additives with perovskite precursor solution (Liang, P. W. et al., 2014). Hu, X. et al., 2015, reported a solution processed planar PSC which allowed perovskite thin films with high surface coverage area to be obtained. By controlling the acceleration and spin time during the deposition of perovskite on the substrate by spin coating, different thicknesses and film morphology can be achieved. A spin time of 5 sec can produce pinholes and voids on the films which result in incomplete surface coverage and non-uniform perovskite thin films making low efficiency planar PSC. As it increases to 10 sec, the fissures are greatly reduced and a uniform perovskite layer with complete surface coverage is formed **(Figure 2.12)**. By increasing the surface coverage, the HTM can have greater contact with the perovskite minimizing shunt path and reduced leakage current (Eperon, G. E. et al., 2014). As the spin time is increased to 20 and 30 sec,

crevices begin to appear on the perovskite film lowering the efficiency. Detailed processing conditions were summarized in **Table 2.2.**

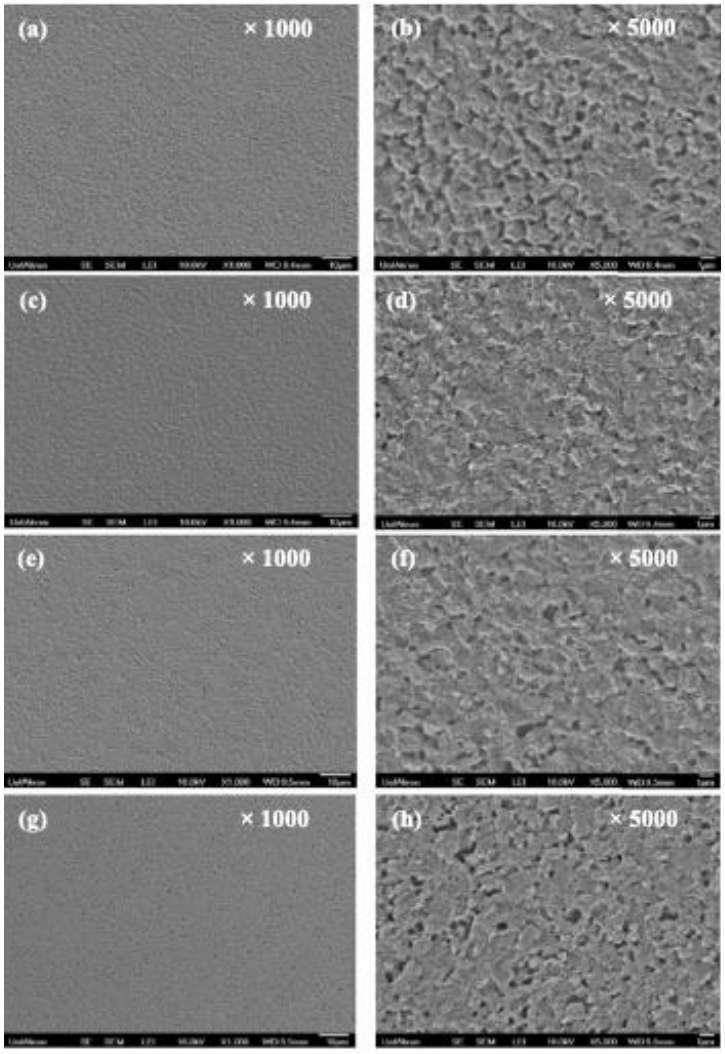

Figure 2.12: SEM images of perovskite films processed at a) and b) 5 sec. c) and d) 10 sec. e) and f) 20 sec. g) and h) 30 sec. (Hu, X. et al., 2015)

Table 2.2: Characterization of Perovskite Films and Devices Performance of Planar PSCs (Hu, X. et al., 2015)

	Processing conditions		Thin film characterization		Device performance parameters			
Devices	Acceleration time (s)	Spin time (s)	Thickness (nm)	Electrical conductivity (S/cm)	V_{OC} (V)	J_{SC} (mA/cm^2)	FF (%)	PCE (%)
A	4	20	580 ± 5		0.85	20.17	61.9	10.61 ± 0.21
B	8	20	577 ± 8		0.85	21.41	62.8	11.43 ± 0.18
C	12	20	580 ± 6		0.85	19.81	60.1	10.12 ± 0.35
D	16	20	580 ± 5		0.85	19.74	59.5	9.99 ± 0.42
E	8	5	600 ± 6	$(4.6 \pm 0.3) \times 10-2$	0.75	18.56	57.5	8.00 ± 0.51
F	8	10	580 ± 4	$(2.0 \pm 0.5) \times 10-1$	0.90	22.59	69.5	14.13 ± 0.16
G	8	20	577 ± 8	$(6.3 \pm 0.4) \times 10-2$	0.85	21.41	62.8	11.43 ± 0.21
H	8	30	570 ± 8	$(5.0 \pm 0.1) \times 10-2$	0.80	20.26	62.7	10.16 ± 0.25

Another study was made to analyze the effects that occurred by altering the thickness and morphology of a $CH_3NH_3PbI_{3-x}Cl_x$ perovskite layer on a planar PSC (Wang, K. et al., 2015). A PSC with structure of ITO/PEDOT:PSS/$CH_3NH_3PbI_{3-x}Cl_3$/$PC_{61}BM$/Al was built by spin coating at different speeds in order to control the thickness of the perovskite layer. More than 50 devices were tested and they found that on average they possessed a similar fill factor (FF) of ~0.61 and V_{OC} of ~0.93 V, but with significantly different J_{SC} which affected the PCEs. They achieved a J_{SC} of 8.45 mA/cm^2 to 19.79 mA/cm^2, then a decrease to 17.26 mA/cm^2 as the thickness was gradually increased from 273 nm to 575 nm, and then further increased to 668 nm, respectively; the PCEs were increased from 4.88% to 11.88% and then decreased to 9.42%, respectively. Thicker perovskite layers had a decrease in J_{SC} due to the inferior surface quality of the films. As the thickness increased above 400 nm, it was found that the efficiency was dependent on the film morphology of $CH_3NH_3PbI_{3-x}Cl_x$ layer. Therefore, in order to achieve high-efficiency PSC, crystallization morphology of perovskite layer must be controlled.

2.3.3.3 Large Scale Fabrication. Most techniques used to fabricate solar cells are impractical for producing large scale PSC. This is an issue that must be resolved in order for

perovskites to replace traditional solar cells. To achieve this, several procedures used for fabrication of small devices need to be scaled over larger substrates such as uniform deposition of layers and the patterning procedures to minimize the contact resistance of the monolithic interconnections (Di Carlo, A. and Matteocci, F., 2015). A new approach was devised called direct contact and intercalation process (DCIP) (Yang, Z. et al., 2015), where a compact TiO_2 layers was deposited on FTO glass by DC magnetron sputter (using Ar as working gas and O_2 as reacting gas) and annealing at 500°C for 1hr in air, followed by spin coating PbI_2 on the TiO_2 layer and annealing at 70°C for 15 mins. CH_3NH_3I powder was spread on a metal container to form a flat layer and pre-heated at 150°C, then the PbI_2 film was placed in direct contact with the CH_3NH_3I powder. The intercalation reaction was done at different time intervals to determine the required time needed to obtain a perovskite layer with better film characteristics. A spiro-OMeTAD solution was spin coated onto the perovskite layer with a gold electrode being thermally evaporated to complete the device. The $CH_3NH_3PbI_3$ films produced by this method were of large grain size, small surface roughness, complete surface coverage, and high reproducibility, meeting the necessary requirements to produce large scale high efficiency perovskite solar cells. The average efficiency obtained for 48 large devices was 10.9% with a top efficiency of 12.6% and a maximum PCE of 16% with an average efficiency of 14.3% for smaller devices.

2.3.3.4 Low Temperature Fabrication. High efficiency PSCs have been achieved using TiO_2 as the ETL that requires annealing at high temperatures (>400°C) in order to form a compact layer which does not allow for low-cost fabrication, devices on polymer substrates, and multi-junction device architecture (Wang, J. et al., 2014). In order to avoid using high temperatures, PEDOT:PSS has been a preferred EBL substitute to TiO_2. It has been proven that a TiO_2 layer can be annealed at lower temperatures to produce high efficiency PSCs. A study was made by

annealing the TiO_2 layer at 150°C creating a mesoporous layer (Dkhissi, Y. et al., 2015). Conventional glass substrates produced efficiencies over 15% and a polymer substrate attained efficiencies exceeding 12%. By combining nanocomposites of graphene nano flakes with TiO_2 nanoparticles, reduced series resistance and recombination loss allow for devices to exhibit up to 15.6% efficiency (Wang, J. et al., 2014). This approach allows new substrates to be considered for the fabrication of solar cells due to their low temperature fabrication.

Annealing temperature greatly impacts the surface morphology, stability, and photovoltaic performance of perovskite solar cells. It is customary to anneal the perovskite films at 90°C for approximately 60 mins but rapid annealing causes fast evaporation of the solvent along with CH_3NH_3I which decreases the device's stability. A new approach, multi-step, for annealing perovskite films was considered where the initial temperature is lower and is increased every 20 mins until reaching 90°C (Huang, L. et al., 2015). Devices that contained perovskite treated with the multi-step slow annealing procedure produced higher efficiencies than those that were annealed in the conventional method. The leading efficiency was 13.58% which was a 57% improvement over those that were not treated with the multi-step due to perovskite layer containing a uniform surface compared to those with pin holes and different size grains obtained from the known procedure. This annealing method is capable of reproducing perovskite films with high crystal quality and good stability.

2.3.3.5 Stability. There are many factors that affects a perovskite solar cell's stability. The fabrication method can also contribute to the device's stability. A layer-by-layer deposition method retained 91% of its initial efficiency after being stored for 62 days under ambient conditions which was believed to be associated to the formation of a dense perovskite layer with full surface coverage preventing moisture penetration (Yang, D. et al., 2015). It has also been shown that the

blade coating method in ambient conditions can improve the stability and photovoltaic performance of a planar PSC (Kim, J. H. et al., 2015) which was attributed to the formation of large crystals and uniform coverage of the perovskite film on the TiO_2 layer. In contrast, devices fabricated by the spin coating method produces devices with lower efficiencies due to the perovskite material degrading. Berson, S. et al., 2007, developed a hybrid vapor phase deposition (HVPV) to grow perovskite layers by a chemical vapor deposition in an inert atmosphere. A top efficiency of 11.8% was achieved with long term stabilities of up to 1100 hrs in a N_2 environment. The high stability is believed to be achieved by using a temperature above 160°C during the fabrication of the film.

It has been noted that solar cells based on $CH_3NH_3PbI_{3-x}Br_x$ tend to have better stability than devices fabricated with $CH_3NH_3PbI_3$ allowing for the solar cell's performance to remain unchanged within 20 days (Noh, J. H. et al., 2013). Different lead precursors used for the perovskite synthesis can impact the stability of PSC. It has been observed that the lead precursor used for fabricating perovskite materials affect the morphology and crystallization of the perovskite layer. Devices fabricated using $Pb(OAc)_2$ as a precursor had similar efficiencies to those prepared with PbI_2, but with lower stability (Dualeh, A. et al., 2014).

The HTM layer above the perovskite layer can protect the perovskite from moisture thus increasing the stability. It has been shown that by replacing the conventional HTM of spiro-OMeTAD, due to its sensitivity to moisture, to a hydrophobic polymer material, the stability can be further improved (Habisreutinger, S. et al., 2014). By incorporating a single wall carbon nanotube instead of the spiro-OMeTAD, PSC had better stability and resistance to moisture. Mei, A. et al., 2014, fabricated a PSC by drop casting a solution of PbI_2, CH_3NH_3I, and 5-ammoniumvaleric acid iodide through a mesoporous carbon film. The device was able to maintain

80% of its initial efficiency after 1008 hrs of use in ambient air which was believed to be due to the hydrophobic nature of the carbon. The strength of hydrogen bonds between the inorganic and organic components of the perovskite material also has a notable impact on its structural stability (Guarnera, S. et al., 2015). Substituting the organic cation of methylammonium with a more polar one has shown an improved stability of the perovskite material (Kim, H. S. et al., 2014; Dong, X. et al., 2015). A device with a TiO_2-ZrO_2 mesoporous layer maintained its efficiency even after 1008 hrs at room temperature (Mei, A. et al., 2014).

2.3.3.6 Simple Structure Devices. PSCs with a simple structure are very appealing due to their low cost and simple fabrication process. A comparison between PSC with and without a PEDOT:PSS layer was made in order to study the change in efficiencies (Wu, R. et al., 2015). A PCE over 11% was achieved via a low temperature, solution process method in an electro-blocking layer (EBL)-free P-PSC. It was noted that the PEDOT:PSS layer only had a ~1% efficiency increase. It was proposed that the high PCE and V_{OC} were caused to the relatively large recombination resistance and low contact resistance in the EBL-free P-PSC. Deng et al., 2014, developed an inexpensive PSC with structure FTO/TiO_2/$CH_3NH_3PbI_3$/P3HT/Ag by modifying the way that the TiO_2 layer was made. An optimal efficiency of 5.15% was achieved by spin coating peroxo titanic acid followed by titanium isopropoxide.

2.3.3.7 Other Methods for Increasing Efficiency. Other methods are being developed to further increase a device's efficiency without altering their structure. An isopropanol treatment was conducted by Wang, X. et al., 2015, which consisted of spin coating anhydrous isopropanol solvent on top of the active layer after the substrate was at room temperature. A PCE of 13.1%

was obtained after the isopropanol treatment, generating a 9% improvement than what had previously been obtained on the untreated device.

Lee, Y. H. et al., 2014, found that the porosity of a mesoporous TiO_2 layer allowed for an enhanced conversion efficiency of PbI_2 to $CH_3NH_3PbI_3$ from exposure of CH_3NH_3I solution. In order to increase the porosity of the mesoporous TiO_2 layer, ZnO nanoparticles were added to the TiO_2 paste and etched under an acidic solution leading to additional mesoporosity in the TiO_2. A 30 wt.% ZnO mesoporous TiO_2 layer was observed to have the highest efficiency of 11.71% providing a new method to further increase the efficiency for mesoporous solar cells.

2.4 Future Work and Challenges

Perovskite materials are capable of producing solar cells with efficiencies of up to 22.1% and it's expected to continue increasing as new fabrication methods and materials are developed. Higher efficiencies have been made possible by modifying a cell's structure with high hopes for perovskite solar cells to replace standard solar cells due to their promising photovoltaic efficiencies and low cost of fabrication. It is worth mentioning that most of the current research has been conducted using a glass/FTO or ITO substrate, TiO_2 or PEDOT:PSS acting as the ETL, $CH_3NH_3PbI_3$ or $CH_3NH_3PbI_{3-x}Cl_x$ as the active layer, spiro-OMeTAD or PCBM as the HTL, and Au or Ag as the cathode to produce high efficiency and low cost perovskite solar cells.

However, there are still some issues that must be addressed before commercialization begins such as their stability and health hazard. To achieve this, better encapsulation techniques and materials with humidity resistance and photo stability must be developed. Another important challenge is developing fabrication methods that have the ability of producing large scale cells with high efficiency, improving the vapor-assisted method would be practical. Lastly, to make

environmentally friendly perovskite solar cells, different elements must be used to replace hazardous materials such as lead. Even though PSCs have shown promising efficiencies, it is crucial to overcome the stability issues in order to produce practical devices. It is important to understand what is involved in the degradation of perovskite materials and develop new methods of encapsulation that can improve their stability in order to commercialize this promising solar cell technology.

CHAPTER III

EXPERIMENTAL SETUP

This chapter discusses the equipment and experimental set up that was used to fabricate and collect the data presented in this thesis. A brief description of the different machines is provided along with their application for the solar cell fabrication.

3.1 Fabrication Equipment

3.1.1 Ultrasonic Bath

Ultrasonic cleaning is a process that uses ultrasound energy and a cleaning solvent in order to remove small particles from materials. It was used in order to remove any particles that were on the substrate, this process is needed in order to prevent impurities within the solar cell's layers. It is also possible to use this system to speed the process of small particles dissolving in a solvent in order to facilitate a solution to become homogenous. Solutions for TiO_2, P3HT, and MAI were sonicated to prevent bigger particles from not dissolving properly.

3.1.2 Magnetic Stirrer with Hot Plate

An adjustable magnetic stirrer with hot plate was used to anneal and evaporate the solvent from the various layers required to complete a solar cell and to homogenize different solutions by stirring them for many hours. Temperatures ranging from 70°C – 150°C were used during the fabrication of the solar cells.

3.1.3 Spin Coater

The dispersion of the layers was applied via spin coating. The solution coating was conducted in two stages. The first stage, at slower speed, allows for the solution to spread throughout the substrate in order for it to be evenly coated and the second stage creates thin layers due to the higher speed that is used. **Table 3.1** shows the different parameters that were used for the different layers that were applied. Some layers were tested using different parameters which are also included.

3.1.4 Sputtering

Sputtering is a process used to deposit thin films of a material onto a substrate. It creates a gaseous plasma and accelerates the ions from the plasma into a target, the material that will be deposited onto the substrate, eroding it from the arriving ions and ejecting it towards the substrate. A direct sputtering system was used to sputter the Ag electrodes on the solar cells where the substrate is positioned directly in front of and parallel to the sputtering source target. In order to prevent the substrate from being fully covered with Ag, a mask **(Figure 3.2)** was used to be able to deposit the desired electrode pattern allowing for certain areas of the cell to be covered with the Ag electrode.

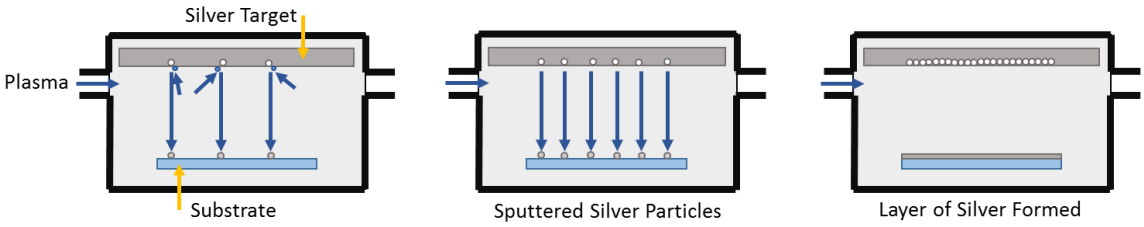

Figure 3.1: Sputtering Process

Table 3.1: Spin Coating Parameters

		1st Stage		2nd Stage			
Material	**Solvent**	**Time (s)**	**Speed (rpm)**	**Time (s)**	**Speed (rpm)**	**Layers**	**Quantity (µL)**
TiO_2	Titanium (IV) isopropoxide, ethanol, distilled water	10 10 10	500 500 500	20 40 60	1000 2000 3000	1	Enough to fully cover the substrate
PbI_2	DMF	10	500	30	3000	1	100
MAI	Isopropanol alcohol	10	1000	10	1000	1	50
P3HT	Chlorobenzene	5	500	20	2000	2	50

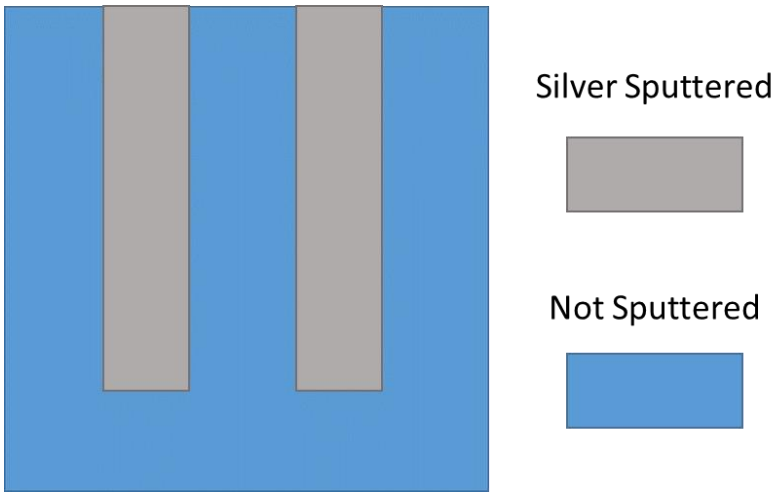

Figure 3.2: Sputtering Mask

3.1.5 Cyclone ForceSpinning™

Currently, electrospinning is one of the most common techniques for nanofiber fabrication but it is only capable of making fibers at a slow rate. ForceSpinning™ is a fiber production method that uses centrifugal forces to produce fibers from polymer solutions. It is capable of producing nanofibers within a few seconds of use whereas electrospinning requires longer times to make the same quantity. A lab scale Cyclone system, manufactured by FibeRio Technology, Inc. was used to fabricate TiO_2 nanofibers by adding the TiO_2 solution listed in **Chapter 4.2** into a cylindrical spinneret with capacity of 1mL with 30 gauge needles attached at the extremities of the spinneret. By spinning the spinneret at 5000 rpm and 7000 rpm fiber were formed within a few seconds and the solution in the spinneret was depleted within 1 minute.

3.2 Characterization and Measuring Equipment

3.2.1 FESEM/EDAX

SEM images were obtained from a Zeiss. It is a type of electron microscope that produces images of a sample by focusing a beam of electrons towards a sample. The electrons interact with the atoms in the sample generating secondary electrons from the sample to go towards the detector, the number of detected electrons changes according to the surface of the sample. By scanning the electron beam and detecting the variation of number of secondary electrons, the surface of the sample can be graphed. It is also possible for the electron beam to ionize the sample atoms making them emit X-rays. With this energy, the chemical composition of the sample can be determined by analyzing the different signals which contain information about the surface of the sample. By increasing the scanning speed better imagery of the sample can be obtained. For the ETL, 6kV-9kV was used in order to obtain better images and 3kV-5kV for the active layer and HTL.

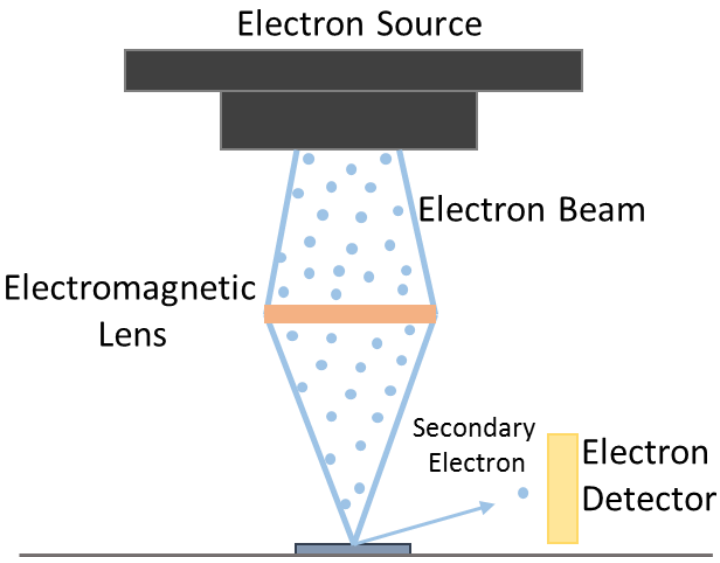

Figure 3.3: SEM Analysis

3.2.2 Solar Simulator for I-V Characterization

The solar cells were measured under standard conditions of irradiance 100 mW/cm^2 with sunlight spectrum at AM 1.5 conditions. It is customary to test solar cells at 25°C but due to not having control over the temperature in the lab, the cells were tested at the temperature that the lab was at which ranged between 65°F - 80°F. A Keithley 2400 source meter was used to measure the I-V curve of each pixel in the devices using a 4 wire test method with 101 steps. The size of one pixel varied between 0.01 cm^2 and 0.1 cm^2 for different devices. The values and calculation of V_{OC}, I_{SC}, *FF*, and *PCE* were obtained from the data in the I-V curve. The solar cells were placed under the solar simulator so the Ag electrode was facing the light source as illustrated in **Figure 3.4**.

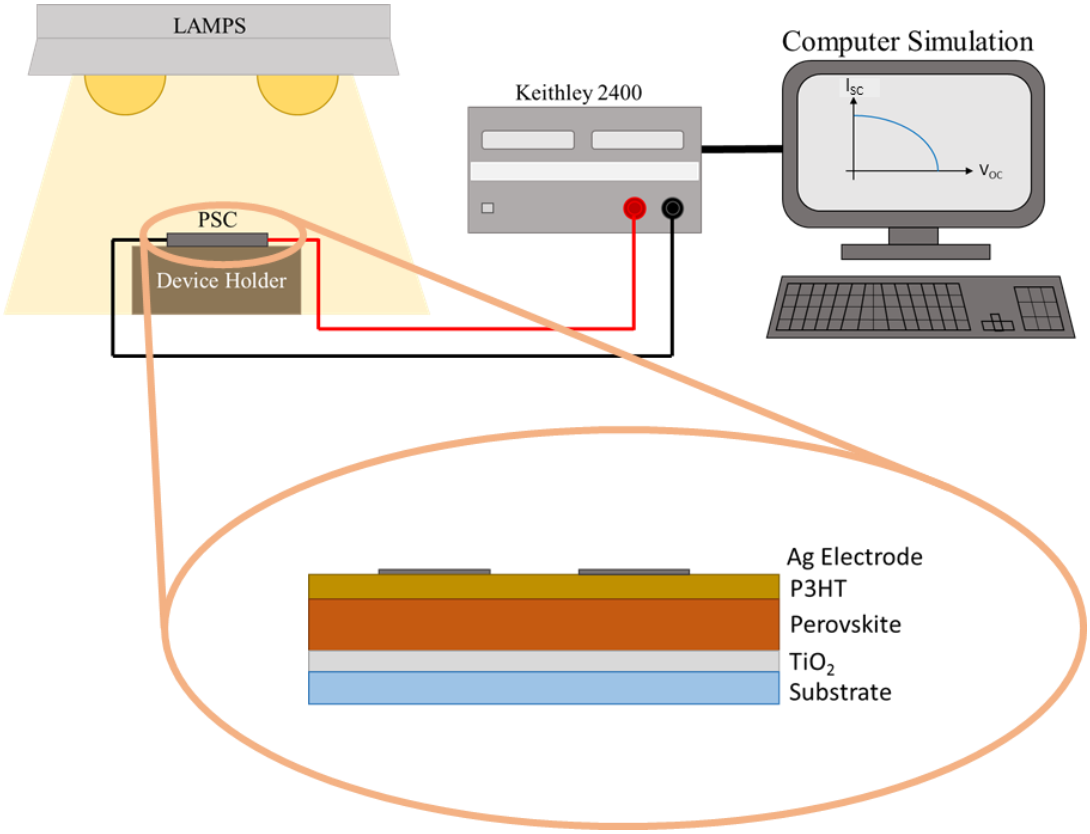

Figure 3.4: Device Testing Setup

CHAPTER IV

EXPERIMENTAL SETUP

4.1 Materials Used

Titanium (IV) isopropoxide (TTIP, 97%, Sigma Aldrich), indium tin oxide coated PET (ITO/PET, 60Ω/sq, Sigma Aldrich), lead (II) iodide (PbI_2, 99.9%, Sigma Aldrich), methylammonium iodide (CH_3NH_3I, MAI, Dysol), Kapton tape (polyimide, 1 Mil, Tapes Master) were purchased and used as received. Poly (3-hexylthiophene-2,5-diyl) (P3HT), poly (vinylpyrrolidinone) (PVP, Mw 1,300,00, Sigma Aldrich), N, N-Dimethylformamide (DMF, anhydrous, 99.8%, Sigma Aldrich), titanium dioxide nanopowder (TiO_2, anatase, 99.7%, Sigma Aldrich), and glacial acetic acid (GAA, >99.7%, Sigma Aldrich) were available in the lab.

4.2 Solution Process

All solutions were made in 10 mL vials and sealed with parafilm to prevent solvent evaporation unless otherwise specified.

TiO_2 – 1 g of TiO_2 nanoparticles were added in 8.5 g of ethanol, 0.159 g of distilled water, and 0.374 g of glacial acetic acid followed by lightly shaking of the vial. After 30 seconds, 0.377 g of titanium (IV) isopropoxide was added to the solution and stirred in a vortex mixer for 60 seconds. The solution was then sonicated for 1 hour and left stirring over night with a stir bar on a hot plate stirrer. Before use, the solution was sonicated for 15 – 30 minutes in order to maintain a homogenous solution.

TiO_2 nanofiber – 0.6 g of PVP was added in 7 mL of ethanol followed by 2 mL of GAA. The vial was stirred in the vortex mixer for 30 seconds. 2 mL of titanium (IV) isopropoxide was added and the color of the solution turned yellow. It was stirred for 60 seconds or until the solution looked homogenous.

PbI_2 – 350 and 400 mg of PbI_2 was added for every 1 mL of DMF and stirred for 3 hours at 70°C on a hot plate until no PbI_2 particles were visible.

Methylammonium Iodide – in a 40 mL vial, 10 and 50 mg of MAI was added for every 1 mL of 2-propanol and left over night until the MAI was completely dissolved or sonicated for 1 hour.

P3HT – 15 mg of P3HT was added for every 1 mL of chlorobenzene and sonicated for 1 – 2 hours until the solution became homogenous.

4.3 Perovskite Solar Cell Fabrication

All of the devices made in this thesis had an inverted structure which requires an electron transport layer to be located on top of the ITO. The active area of a single cell is defined by the overlap between the cathode and anode as illustrated in **Figure 4.1** defined in the red area, or by the area of the opening in a mask.

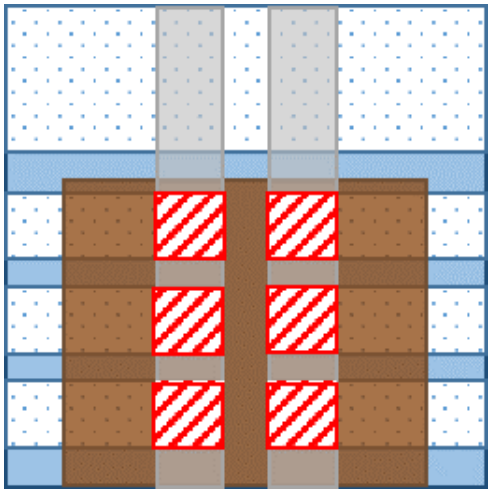

Figure 4.1: Active Area of PSC

The solar cell fabrication begins with a transparent substrate coated with a conductive transparent layer. PET/ITO is used for this research and we begin by etching part of the ITO from the substrate in order to prevent the solar cell from shorting. Two different methods were used to achieve this. The first method, the substrates were covered with pieces of Kapton tape with a desired pattern which determines the location of the anode and cathode of the solar cell. With a cotton swab that contains a diluted HCl solution, the ITO was removed from the substrate in the areas not covered with Kapton tape. The second method, once the substrates were covered with Kapton tape, they are submerged in a bath of diluted HCl with zinc pellets and sonicated for 5 minutes where the zinc allowed for a faster reaction between the HCl and ITO to occur. After etching, the PET/ITO substrate was cleaned via ultrasonic bath in a soap solution, acetone, isopropanol alcohol, and distilled water for 5 minutes each. The devices were blown dry with compressed air for 1 minute. Different patterns for the electrodes were used shown in **Figure 4.2** in order to compare the results and determine which produced better.

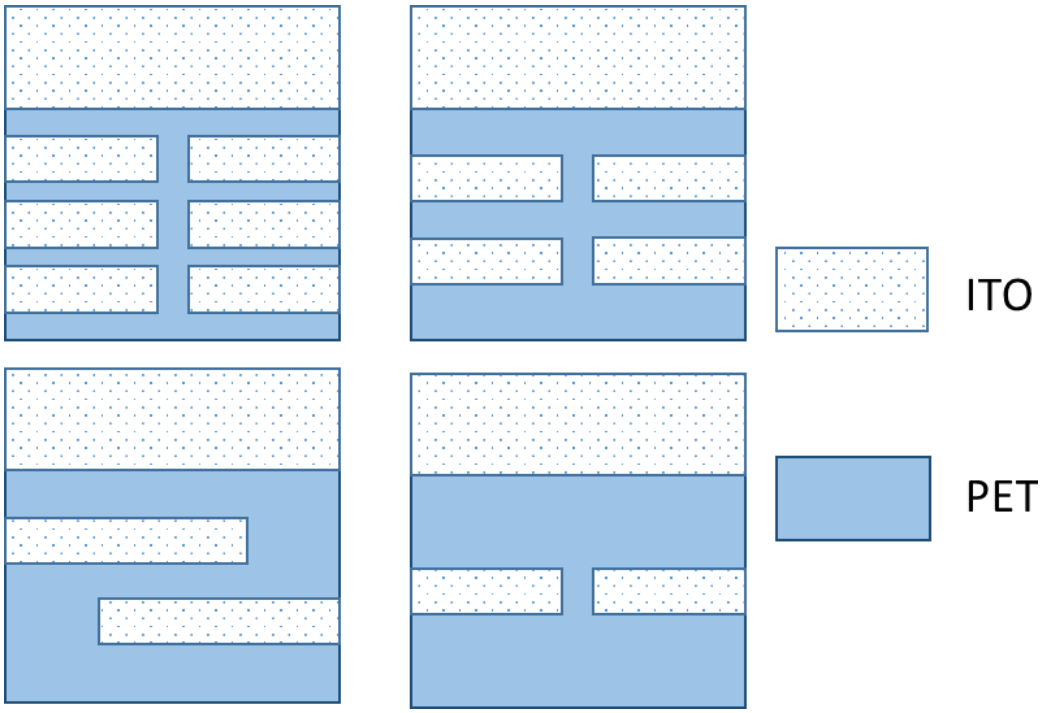

Figure 4.2: Substrate Etching Results

Once the substrates have been etched and cleaned, the solution for the electron transport layer (TiO_2) is applied via blade coating or spin coating. When blade coating the layer, Kapton tape is applied on the edges of the substrate and blade coated with a glass stirring rod and the excess TiO_2 solution is removed with a cotton swab. When spin coating, the substrate is fully coated with the TiO_2 solution before being spin cast with the parameters shown in **Table 3.1**. It is then annealed in a hot plate with temperatures ranging between 120°C - 150°C for 1 to 4 hours. The temperature is then reduced to 70°C before spin coating the PbI_2 layer with parameters shown in **Table 3.1**. It is then annealed at 70°C for 10 minutes to fully remove the solvent. The MAI layer is then deposited either by spin coating with parameters shown in **Table 3.1** or by submerging the PbI_2 coated substrate in a vial containing the MAI solution for 10 minutes. After the time has passed, the substrate is cleaned of the excess MAI solution by gently tapping it with a laboratory

wipe. It is then annealed at 90°C for 30, 60, or 90 minutes or at 130°C for 100 seconds. Once the substrate is slowly cooled to room temperature, the hole transport layer (P3HT) is deposited with the parameters in **Table 3.1**. The silver electrode is then sputtered for a total time of 2 – 3 minutes and are stored in a container with silica bags to prevent them from being exposed to high humidity levels until they are ready to be tested and characterized. **Figure 4.3** and **4.4** show the steps take while fabricating the solar cell and a diagram with the major processes that were taken.

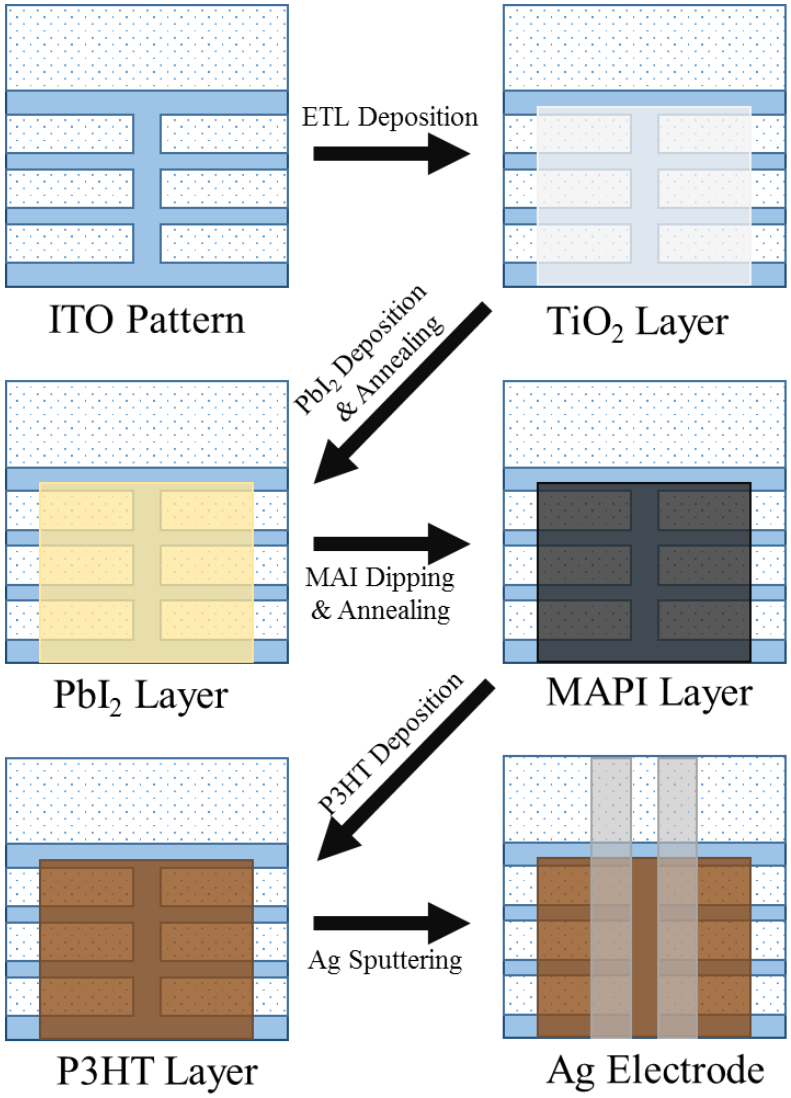

Figure 4.3: PSC Layer Deposition Steps

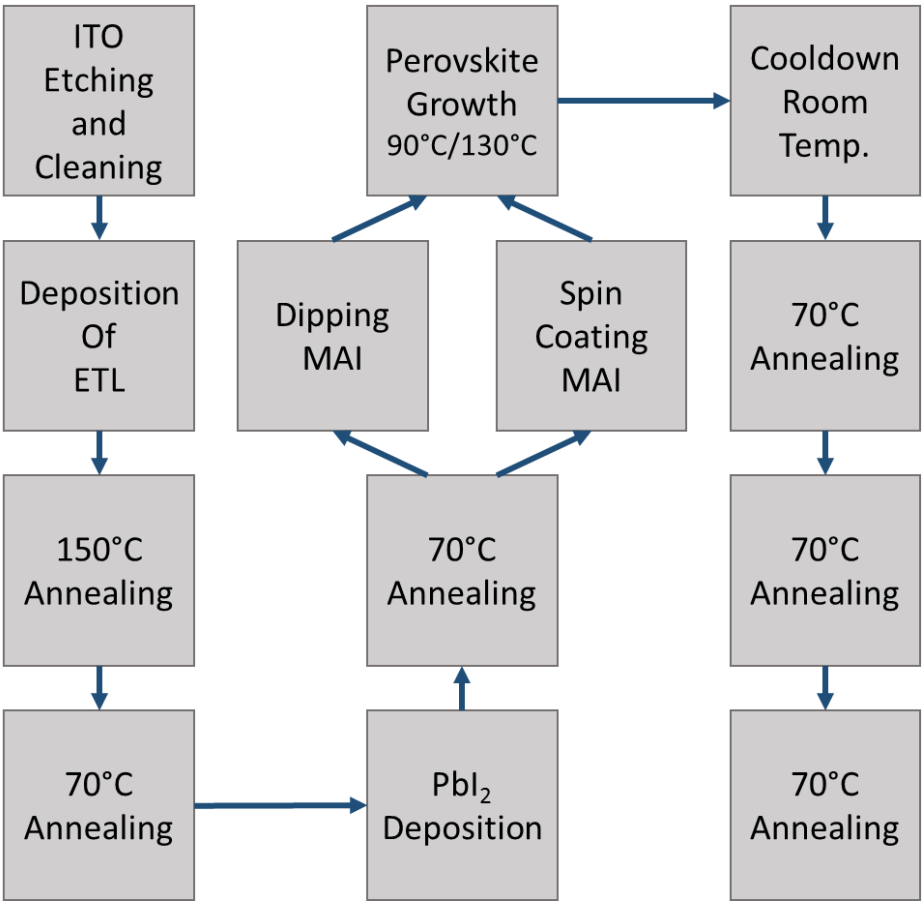

Figure 4.4: Overview of Major Processes for PSC Fabrication

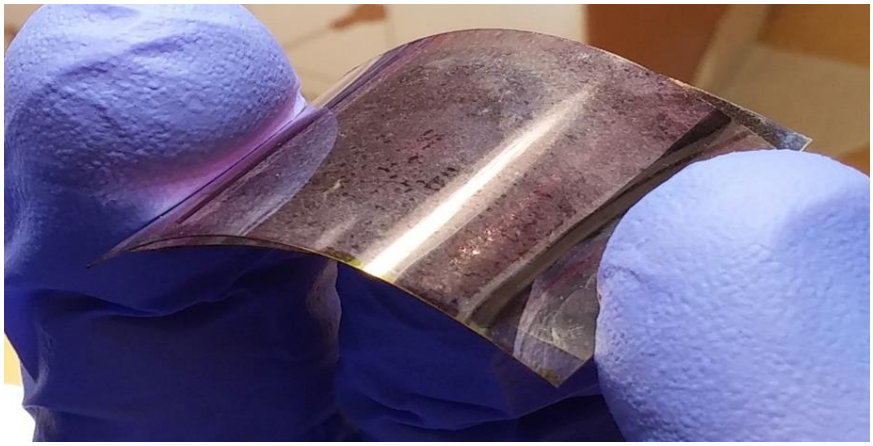

Figure 4.5: Completed Flexible PSC

4.4 Solar Cell Characterization Parameters

In order to characterize the performance of a solar cell, several parameters are needed in order to calculate the efficiency of the solar cell which are as follows: open-circuit voltage (V_{OC}), short-circuit current (I_{SC}), peak power (P_{max}), and fill factor (FF). These parameters can be obtained from the I-V curve **(Figure 4.6)**. The efficiency (η) can then be calculated using the parameters. To understand these parameters, a brief explanation is given below for a simple p-n junction solar cell.

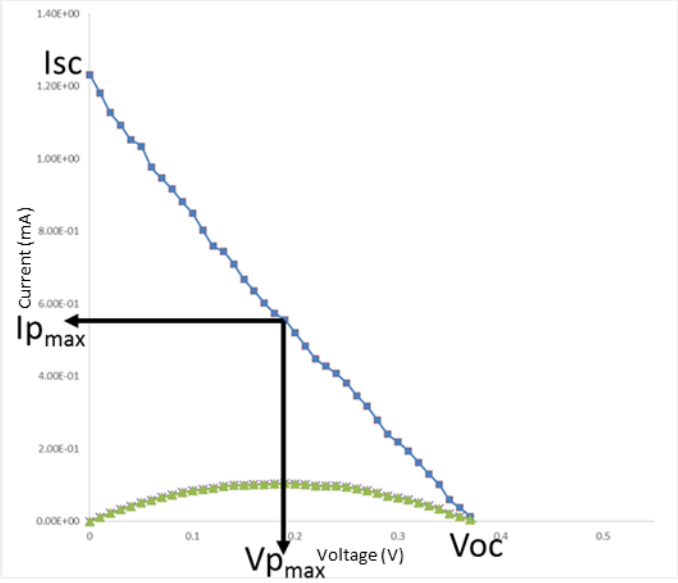

Figure 4.6: I-V Curve

4.4.1 Short-Circuit Current (I_{SC})

The short-circuit current is the current flowing through the solar cell when the voltage across the solar cell is equal to zero (i.e. the electrodes of the solar cell are short circuited). It is the most current which can be drawn from the solar cell which it is directly dependent on the

intensity of the light. The I_{SC} can be obtained from the net current *I(V)* in the solar cell given as (Zeman, M.)

$$I(V) = I_{SC} - I_{dark}\,(V) \tag{4.1}$$

where $I_{dark}(V)$ is the dark current given by

$$I(V) = I_0\left(e^{\frac{qV}{mKT}} - 1\right) \tag{4.2}$$

The behavior of the solar cell is described with the equation (4.2) for an ideal diode with an additional current source I_{SC} when it's under illumination. Using the elemental electron charge $(q = 1.603\ x\ 10^{-19}\ C)$ and Boltzmann's constant $(K = 1.38\ x\ 10^{-23}\ JK^{-1})$, the illuminated solar cell is represented as

$$I(V) = I_{SC} - I_0\left(e^{\frac{qV}{mKT}} - 1\right) \tag{4.3}$$

thus the short circuit current is given by

$$I = I(V) + I_0\left(e^{\frac{qV}{mKT}} - 1\right) \tag{4.3}$$

where V is the voltage across the junction, I_0 is the dark saturation current, m is the ideality factor with values between 1 and 2, and T is the absolute temperature (Zeman, M.).

4.4.2 Open-Circuit Voltage (V_{OC})

The open-circuit voltage is the voltage at which no current is flowing through the external circuit. It is the maximum voltage that the solar cell can output. The V_{OC} is dependent on the light-

generated current, I_L and can be calculated from equation (4.1) if we assume that the net current is zero (Zeman, M.).

$$V_{OC} = \frac{mKT}{q} \ln\left(\frac{I_L}{I_0} + 1\right) \tag{4.4}$$

Equation (4.4) was obtained from equation (4.3) by setting the net current to zero. The compensation effect between the dark and illuminated current takes effect such that $I(V) = 0$, $I_L = I_{SC}$, and $V = V_{OC}$.

4.4.3 Fill Factor (FF)

The V_{OC} and I_{SC} are the maximum voltage and current, respectively, from a solar cell. At these operating points, the solar cell does not have output power. The fill factor is defined as the ratio of the maximum power $(P_{max} = V_{mp} \times I_{mp})$ from the solar cell to the product of V_{OC} and I_{SC} represented as

$$FF = \frac{P_{max}}{V_{OC}I_{SC}} = \frac{V_{mp}I_{mp}}{V_{OC}I_{SC}} \tag{4.5}$$

were V_{mp} and I_{mp} are the maximum point voltage and current generated by a solar cell. The *FF* is a measure of the 'squareness' of the I-V curve, with a higher voltage, a higher *FF* can be achieved (Green, M. A., 1981).

4.4.4 Power Conversion Efficiency (η)

Efficiency is defined as the ratio between the energy output from a solar cell to input energy from the sun represented as

$$\eta = \frac{P_{max}}{P_{in}} = \frac{V_{mp}I_{mp}}{P_{in}} = \frac{V_{OC}I_{SC}FF}{P_{in}} \tag{4.6}$$

It shows the performance of a solar cell, it is dependent on the spectrum, intensity of the incident sunlight, and temperature of the solar cell (Green, M. A., 1981). In order to be able to compare different solar cells, the condition in which they are tested must be the same. Terrestrial solar cells are tested under irradiation of 100 mW/cm^2 with sunlight spectrum of AM 1.5 conditions at temperature of 25°C. P_{in} is determined by multiplying the incident radiation flux with the area of the collector. Thus the efficiency can also be represented as

$$\eta = \frac{P_{max}}{F(incident\ radiation\ flux) * A_C(area\ of\ collector)} \tag{4.7}$$

CHAPTER V

RESULTS

This chapter discusses the results that were obtained during the PSC characterization and experimentation.

5.1 Layer Characterization

Layer morphology is affected by many variables including the concentration of the solution, spin coating speed and time, annealing temperature and time of the substrate, and humidity of the room. This section will focus on the effects that occurred to the layer morphology when different variables were involved. Scale on images taken during EDAX analysis are not correct.

5.1.1 Mesoporous TiO_2 Electron Transport Layer

Initially a TiO_2 NP with ethanol paste was made that had the consistency of toothpaste. It was then blade coated by applying a mask of kapton tape on the substrate and enough paste to cover the substrate when the testing rod was rolled across. After annealing at 90°C for 40 mins, SEM images were obtained in order to observe the deposition of the ETL. As shown in **Figure 5.1**, the TiO_2 layer was not smooth or covering the whole substrate. The layer contained large concentrations of TiO_2 NP that had diameters greater than 100 µm. It was also noticeable that the ETL contained many large areas where the substrate was not covered with TiO_2.

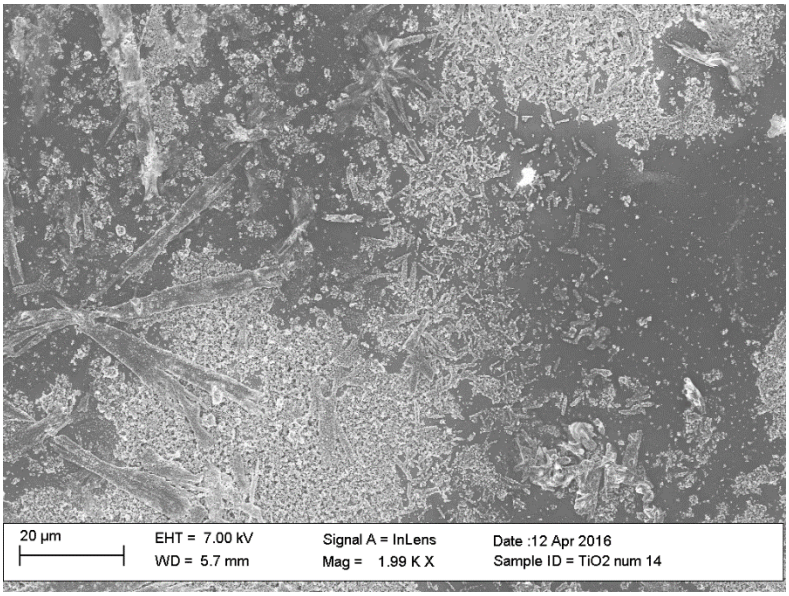

Figure 5.1: Initial TiO_2/Ethanol Paste Deposition

In order to improve the ETL, a less viscous solution was needed to improve solution dispersion as well as experimentation with different deposition techniques. Different concentrations of TiO_2 NP and ethanol was used until a less viscous solution was made and improvements on the ETL were noticeable. Unfortunately, the ETL still contained large areas that were not coated and many TiO_2 NP formations were still visible. In order to improve this issue, a solution with TTIP, distilled water, and acetic acid was needed in order to fully cover the substrate with a TiO_2 layer due to TTIP reacting with water to form TiO_2 (Hanaor, D. A. et al., 2012). The solution concentration is listen in **Chapter 4.2**.

Blade coating, spin coating, and spray coating was used to deposit the new solution for the ETL in order to compare the layer's morphology with the different deposition techniques. Due to the spray coating not giving good results in the layer deposition **(Figure 5.2)** no further testing was performed. Depositing the solution via blade coating seemed to produce smoother layers **Figure 5.3** than by spin coating but it still contained large formations of TiO_2 NP and gaps were

visible on the layer. After EDAX analysis on the gap area, it was observed that the gaps were not coated with TiO_2 which should have been synthesized by the TTIP and water after the annealing of the substrate.

Spin coating was making smoother layers than when the TiO_2 paste was initially used but it was less than blade coating. It contained less holes and they were smaller in diameter. It also contained less and smaller TiO_2 formations when using solution TiO_2 (2). In order to attempt to fill in those gaps, 2 layers were deposited on the substrate by spin coating which showed an improvement when it came to coating the substrate but the layer was not as smooth as previously done with 1 layer **Figure 5.4**.

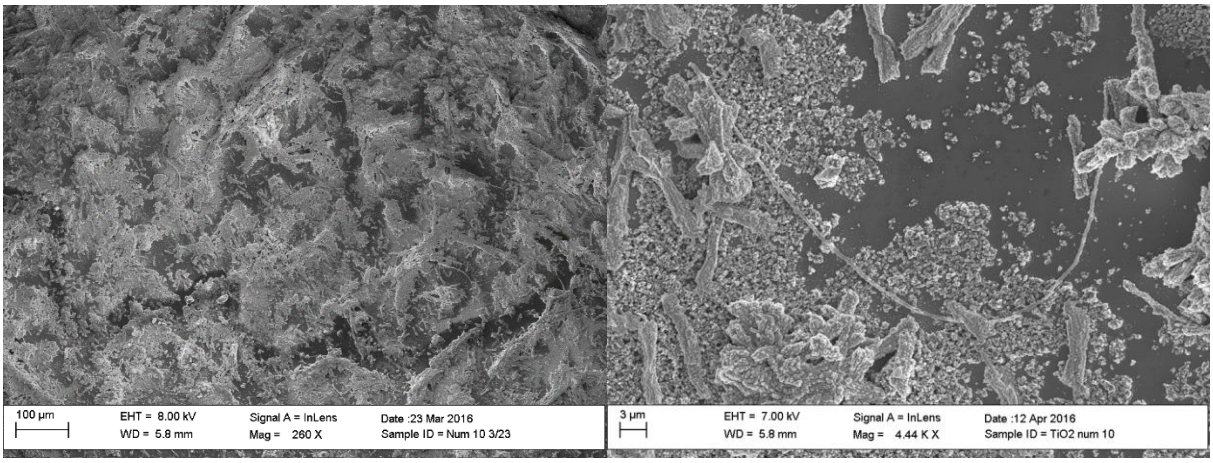

Figure 5.2: Spray Coated TiO_2 Layer with Small Areas of Perovskite

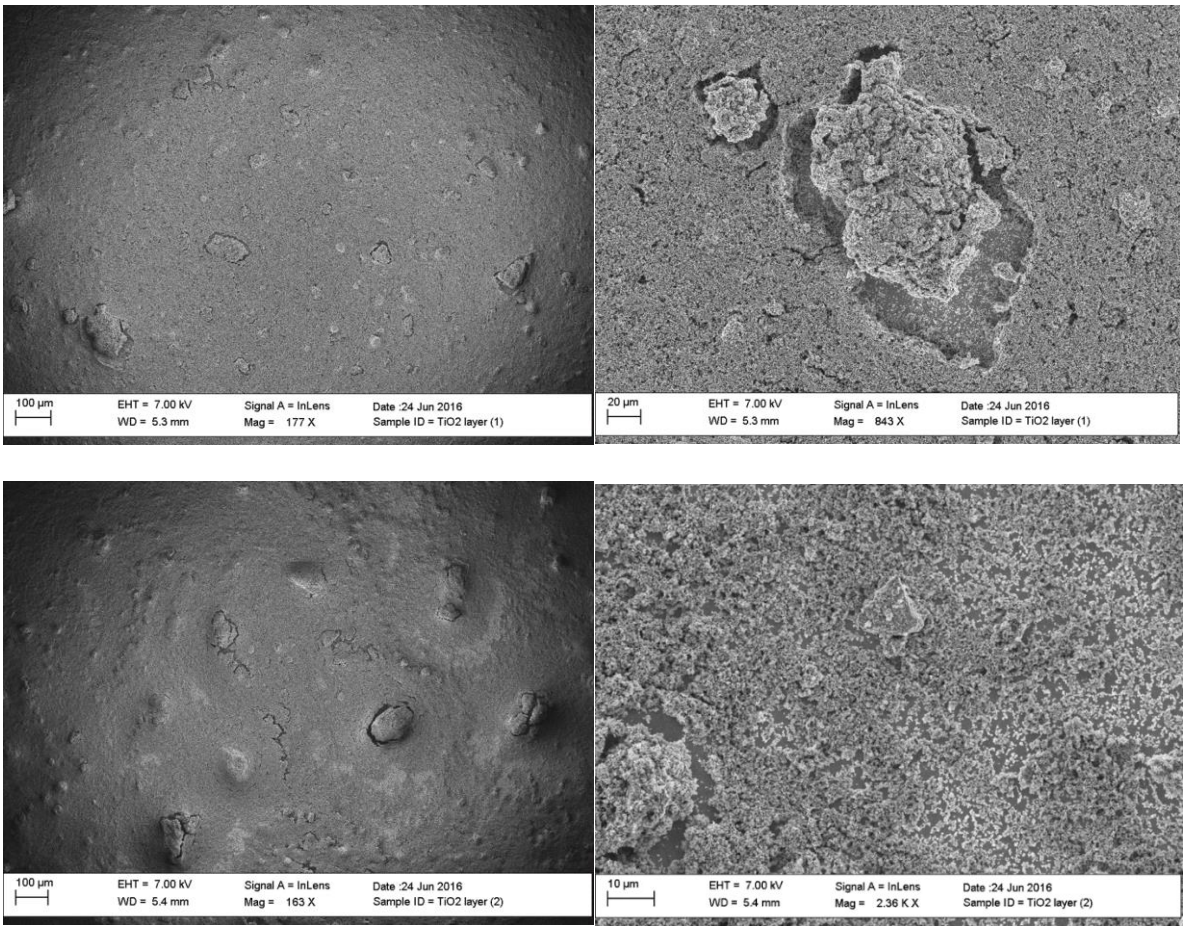

Figures 5.3: TiO_2 Solution (2) A and B. Blade Coated and C and D. Spin Coated 1 Layer

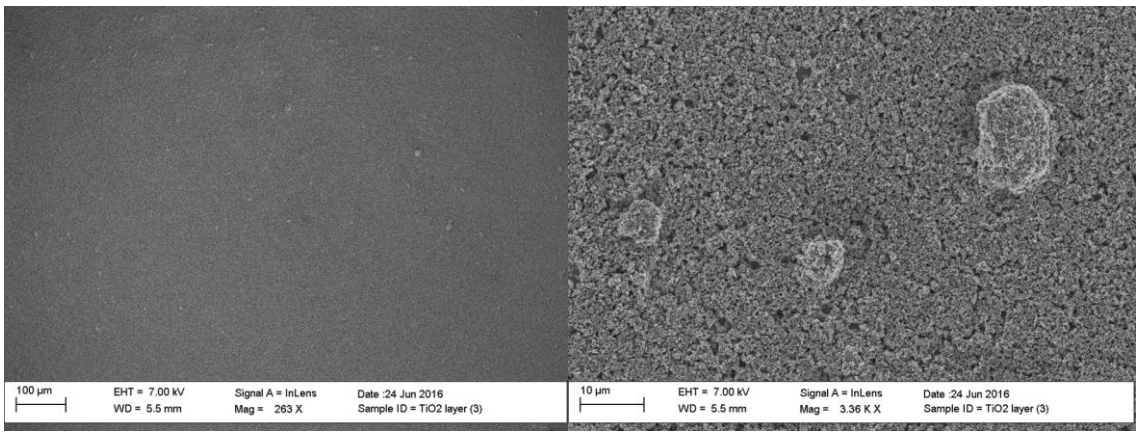

Figure 5.4: Solution (2) Spin Coated A. 1 layer and B. 2 layers

A different ETL solution concentration was made in order to compare the layer morphology with that of solution TiO_2 (2). When using solution TiO_2 (1), the ETL layer had a smoother surface when using this solution for both spin coating and blade coating techniques (**Figure 5.5)**. TiO_2 NP formations were still visible but there were less than with previous solutions. They had sizes approximately 2 µm and 10 µm in diameter for blade coating and spin coating, respectively. After EDAX analysis on the small gaps, it was observed that they were covered with TiO_2 **Figure 5.6**.

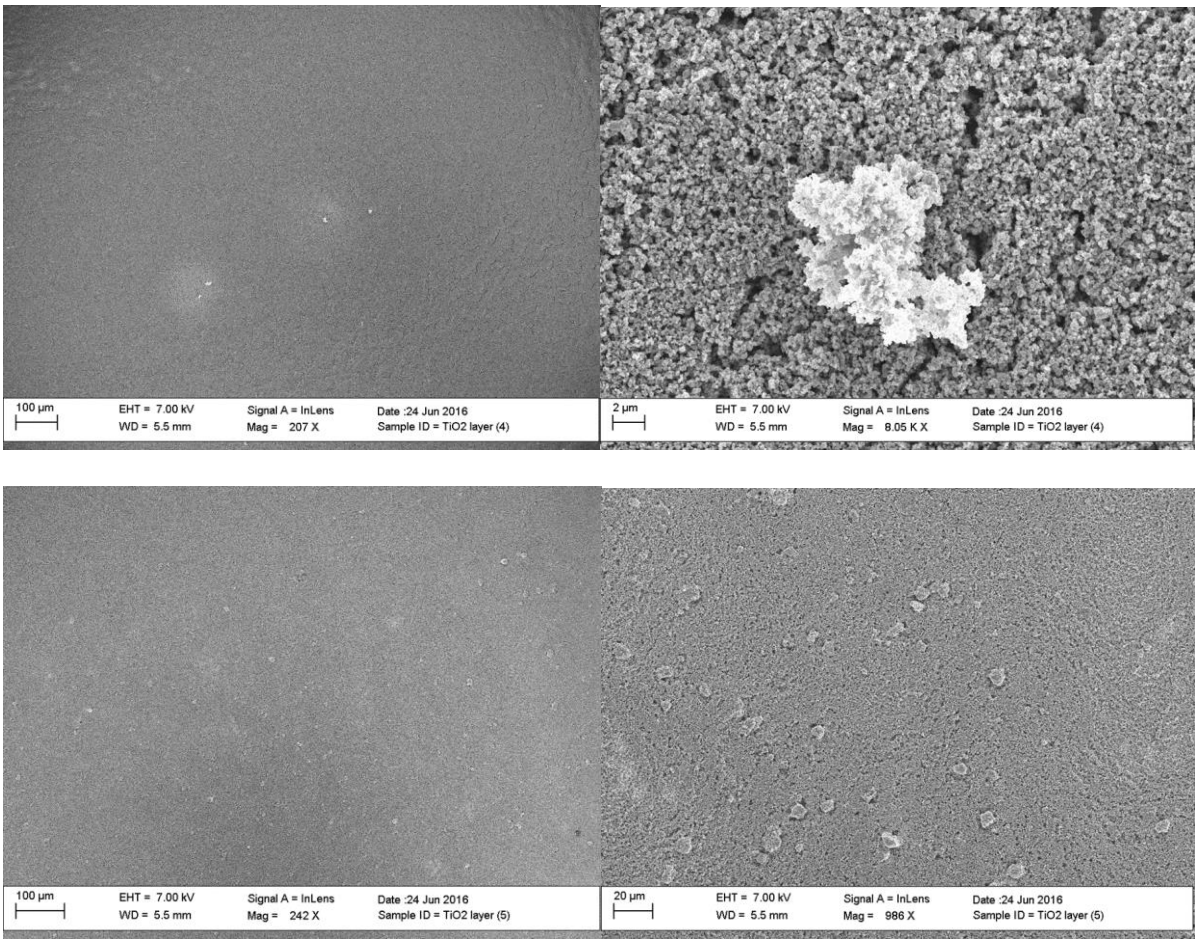

Figures 5.5: Solution (1) A. Blade Coated and B. Spin Coated

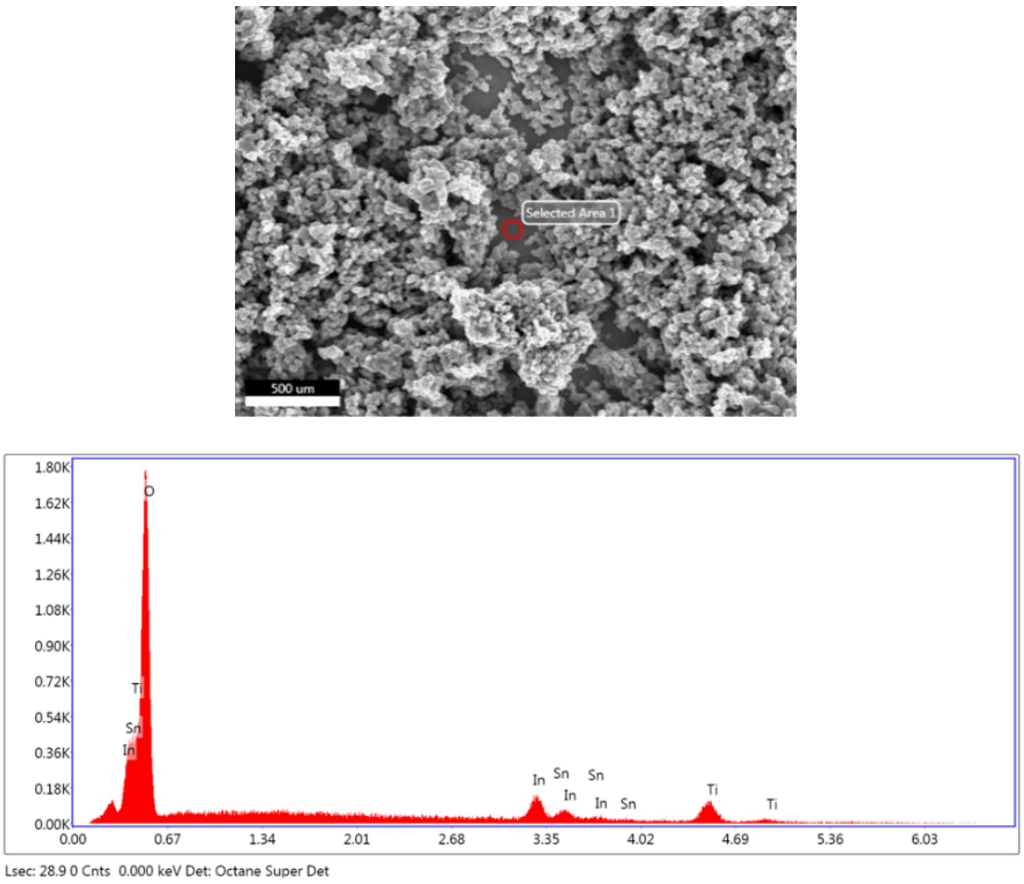

Figure 5.6: ETL gap used for EDAX and results showing TiO_2 on the gaps

5.1.2 Perovskite Active Layer

Perovskite layers were difficult to grow on the ETL composed of the TiO_2/ethanol paste. Only small patches of the ETL were covered with perovskite as shown in **Figures 5.7**. This could have been caused due to the imperfections on the ETL layer not allowing the PbI_2 solution to spread evenly throughout the substrate because of the large TiO_2 formations and gaps within the layer thus the perovskite layer not being able to form properly.

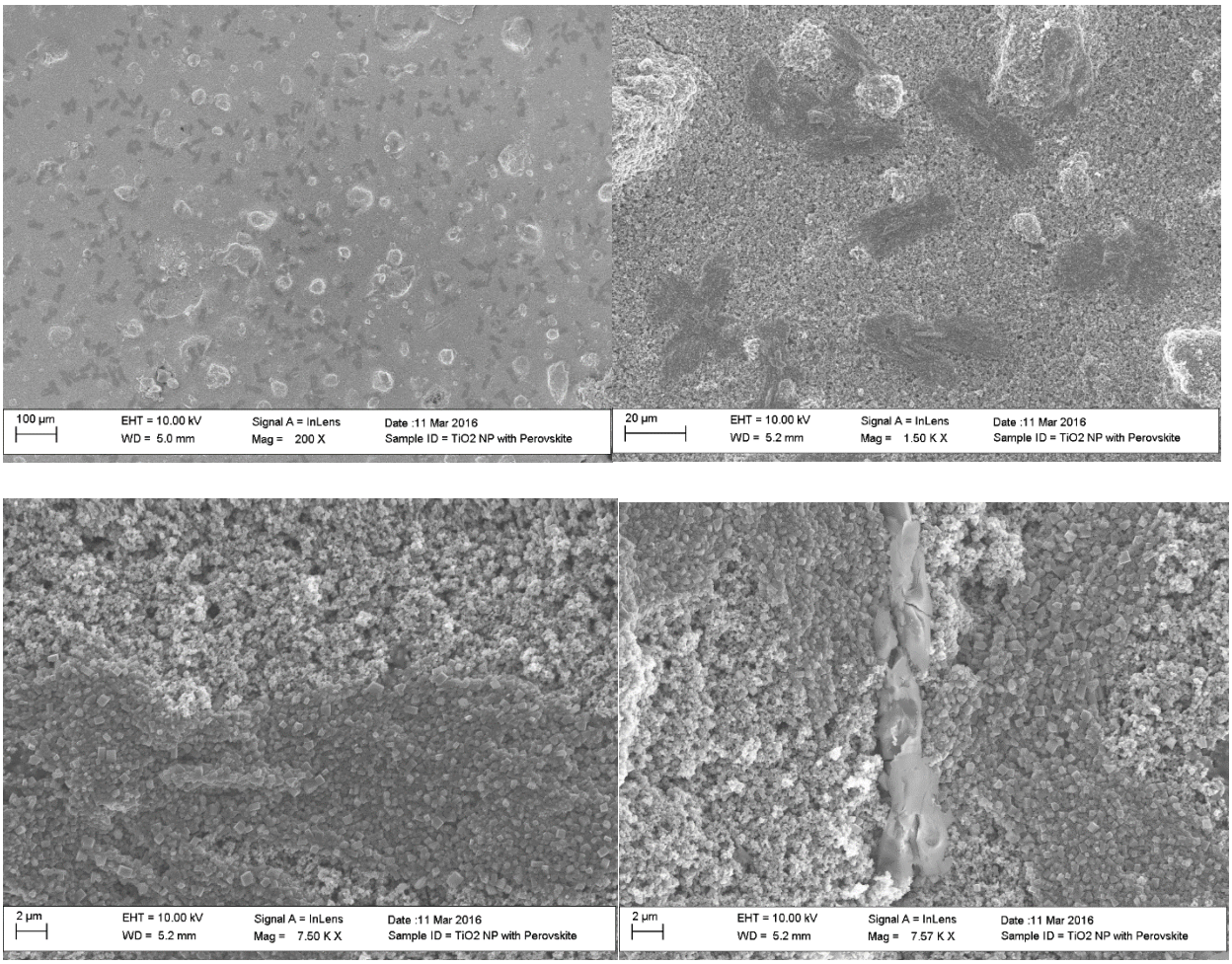

Figure 5.7: Small Patches of Perovskite on ETL

Once the new TiO_2 solution was used, the perovskite layers started forming more uniformly. Unfortunately, there were many gaps within the layer which affected the efficiency of the cells. Using different speeds for the ETL deposition and different annealing temperature and time also seemed to affect the way that the perovskite layer was forming. When using higher speeds (3000 rpm) with lower annealing temperature (90°C) and longer time (60 – 90 mins), the perovskite layer formed more uniformly throughout the substrate **(Figure 5.8)**. It seemed to form in a fibrous mesh manner throughout the layer which caused it to contain pinholes. Slower speeds (1000 rpm) with higher annealing temperature (130°C – 150°C) and shorter time (90s) produced

an uneven perovskite layer that had large fibrous formations **(Figure 5.9)** that were ~15µm long. The grains had an average size of 539nm in diameter.

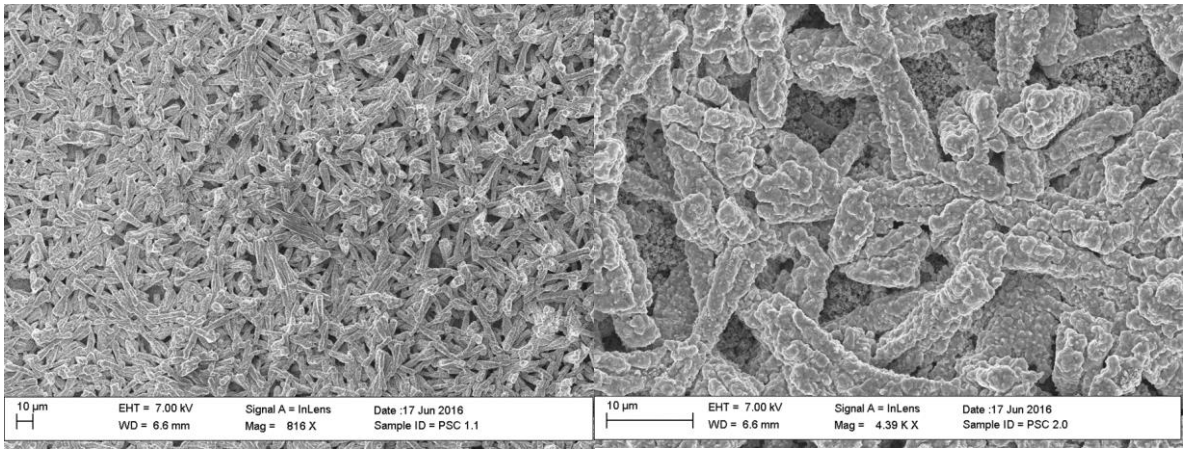

Figure 5.8: High Speed with Low Temperature/Long Time Annealing of Perovskite Layer

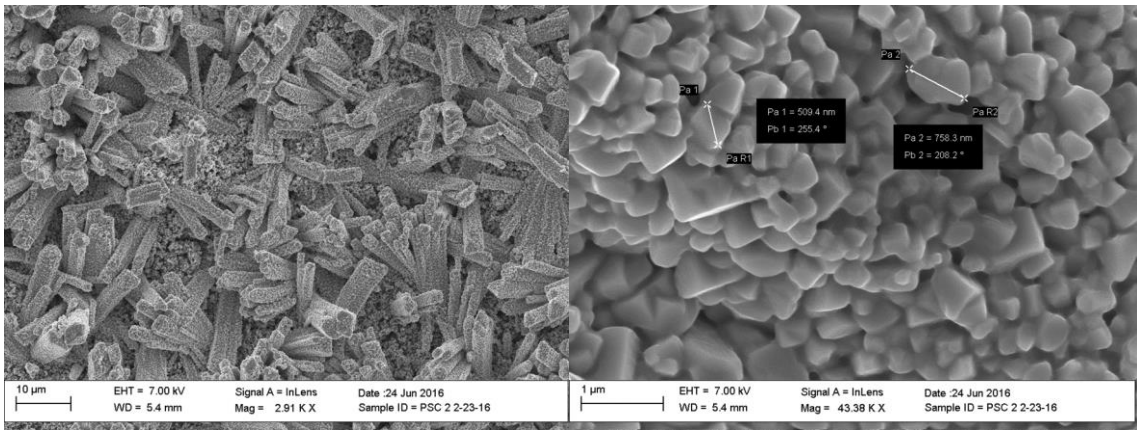

Figure 5.9: Low Speed with High Temperature/Short Time Annealing of Perovskite Layer

TiO_2 nanofibers were also fabricated through Forcespinning^{TM} using the solution in **Chapter 4.2**. When the lab humidity was between 30 – 45% with temperatures of 75 – 82°F, mats were able to be generated using 10mL of solution. After the humidity increased by 30% and

temperature decreased by 10°F, fiber production decreased dramatically. In order to produce fibers once again a different concentration, listed in **Chapter 4.2**, was made using glacial acetic acid. Even after the modification in concentration, fiber production was not as efficient as it was with the initial lab conditions. The TiO_2 NF were annealed in a furnace at 550°C for 4 hrs in inert atmosphere. EDAX analysis was performed to compare acetic acid with glacial acetic acid in TiO_2 NF production. **Table 5.1 and 5.2** shows the difference in element percentage that the fibers had with the different acids. Fibers produced with glacial acetic acid contained twice the amount of titanium and half the amount of nitrogen.

Table 5.1: Element Percentage in Fibers Made with Acetic Acid

Element	Weight %	Atomic %	Net Int.	Error %
C	42.96	51.68	1,331.74	4.68
N	14.73	15.19	133.23	12.66
O	33.86	30.58	654.70	9.47
Ti	8.45	2.55	85.92	10.07

Table 5.2: Element Percentage in Fibers Made with Glacial Acetic Acid

Element	Weight %	Atomic %	Net Int.	Error %
C	43.85	56.04	733.23	5.10
N	7.57	8.30	37.06	15.08
O	31.44	30.17	317.43	10.18
Ti	17.13	5.49	96.07	10.55

5.2 PSCs Performance

The initial ETL deposition method of blade coating a TiO_2/ethanol paste was giving output voltages ranging between 0.1 mV – 5 mV. This can be accountable to the ETL not being deposited properly. It contained many large areas that were not covered with TiO_2 and the perovskite layer was not forming properly due to the imperfections within the ETL. After the TiO_2 paste was improved and made less viscous with a concentration of 1:5 of TiO_2 NP and ethanol, the cells were producing higher output voltages between 40 mV – 80 mV. The voltage was still low because the ETL still contained many imperfections and the perovskite layer was only covering small areas throughout the layer. The cells were stored in the lab with humidity levels up to 45% and

temperature of 66°F. These cells were tested again after 3 days had passed and they produced higher output voltages. The output voltage increased to 100 mV – 180 mV.

By applying 2 layers of PbI_2 at 3000 rpm, the cells output voltage increased and were more stable. PSCs 2 and 3 contained 2 layers of P3HT and PSCs 1 and 4 contained 3 layers. The cells that contained 2 layers of P3HT produced lower V_{OC} with higher I_{SC} and FF than those with 3 layers. These cells were tested using the solar simulator and their efficiency was calculated using the formulas in **Chapter 4.4** which are shown in **Table 5.3**. Spin coating of PbI_2 was decreased to 2000 rpm for 20s to see how the cell would be affected. The V_{OC} increased to 326 mV and remained constant after 1 day of being stored in air with 43% humidity.

Table 5.3: Efficiency of Early PSCs

PSC	Active Area (cm^2)	V_{OC} (V)	I_{SC} (mA)	FF	Efficiency (%)
1	0.25	0.284	7.03E-3	0.15	1.20E-3
2	0.3	0.262	1.26E-2	0.25	2.75E-3
3	0.12	0.183	4.20E-2	0.23	1.47E-2
4	0.25	0.285	1.11E-3	0.19	2.40E-4

Using the solution in **Chapter 4.2** for the ETL, different HTM depositions were compared. A PSC was fabricated with a P3HT HTL that had 1 layer of 80 µL which was spin coated at 500rpm for 1 s and 2500rpm for 25 s and another that had 2 layers of 40 µL spin coated at 500rpm for 5 s and 1000rpm for 25 s with all of the other processes remaining the same. The PSC that had 1 layer of P3HT only had a V_{OC} of ~25 mV and the PSC with 2 layers had a maximum V_{OC} of 750 mV. This proved that applying 2 layers of P3HT for the HTL did produce higher efficiency for the PSCs which is due to the second layer of P3HT covering any gaps that were not initially covered with the first layer preventing a short to occur within the cell.

There was an increase in humidity levels in the lab which ranged between 55% – 58% which affected the performance of the cells. The cells were tested immediately after being made and they had an initial V_{OC} of ~370 mV but within a couple of hours they decreased to approximately 62 mV. PSCs that had been made with humidity levels below 46% were capable of maintaining their performance for a few days before degrading. It was observed that the Ag electrode began to oxidize faster than it had previously done so which is believed to be a factor for the decrease in V_{OC} of the PSC over time. During the MAI deposition the PbI_2 layer would have some areas that turned dark brown/black within 30 s. After 10 mins had passed, there were still areas that had not been converted and stayed yellow indicating that there were areas that only contained PbI_2. This could have occurred due to the decrease in speed for the PbI_2 deposition which did not allow the solution to form an even layer.

New PSCs were annealed at 130°C for 30, 60, 90, and 120 s whereas previous PSC were annealed at 90°C for 60 – 90 mins. The PSCs that were annealed for 30, 60, 90, and 120 s had an average V_{OC} of 150 mV, 310 mV, 216.5 mV, and 395 mV with an average voltage drop of 35.6 mV, 198 mV, 71.5 mV, and 178.6 mV, respectively, after 10 mins of fabrication. PSCs that were

annealed for 30 s had a lower voltage decrease compared to the other cells but annealing for 90 s was chosen due to the higher obtained voltage after the degradation of the PSCs. Different concentrations of PbI_2 (250, 300, 350, 400 mg ml^{-1}) in anhydrous DMF were used to fabricate the four PSCs with a 0.01 cm^2 mask in order to determine the concentration that would produce the best results. The 250 mg ml^{-1} produced V_{OC} = 504 mV, I_{SC} = 3.58E-3 mA, and FF = 0.25. The 300 mg ml^{-1} produced V_{OC} = 588mV, I_{SC} = 4.55E-3 mA, and FF = 0.24. The 350 mg ml^{-1} produced V_{OC} = 637 mV, I_{SC} = 7.69E-3 mA, and FF = 0.24. And the 400 mg ml^{-1} produced V_{OC} = 511 mV, I_{SC} = 6.30E-3 mA, and FF = 0.26. It took approximately 10 – 15 mins for the voltages to reach their maximum point and they degraded completely after 1 hr. of exposure to the humid lab environment. It was also observable that the Ag electrode had oxidized and contained many holes. Using a PbI_2 concentration of 350 mg ml^{-1} produced higher V_{OC} and I_{SC} than the other concentrations but a lower FF than the concentration of 400 mg ml^{-1}. Following the same processing of annealing the substrate at 130°C for 90s to form the perovskite layer, new cells were made and tested without masking and recorded on **Table 5.4**. These new cells had an improved I_{SC} than previously made cells and a maximum V_{OC} and I_{SC} were obtained.

Initially after cleaning the substrates, they would be removed from the cleaning solution, dried with a lab cleaning wipe which would leave tissue residue and scratches on its surface, and masked with kapton tape. The substrates would then be placed near the spin coater to be applied with the ETL solution which could allow for dust particles to fall on them before the deposition of the layers. The impurities within the substrate and the poor ETL deposition caused the PSCs to have low I_{SC} ranging between 1E-4 mA to 8E-3 mA. A better method for cleaning the substrates was then performed by sonicating the substrates in the cleaning solutions for 5 – 10 extra mins, leaving them in the cleaning solution until they were going to be needed for the ETL deposition to

prevent particles within the lab to fall on them, and dried with air flow to prevent scratches on the substrates. Once a better cleaning procedure was followed, a new ETL solution **(Chapter 4.2)** was developed and the spin coating parameters were altered, an improved layer morphology was obtained allowing for higher I_{SC} to be obtained on new cells. The improved cells had a I_{SC} ranging from 1E-1 mA to 1.3 mA allowing for higher efficiencies to be obtained (**Table 5.5)**.

Table 5.4: PSCs with New Perovskite Layer Processing

PSC	Active Area (cm^2)	V_{OC} (V)	I_{SC} (mA)	FF	Efficiency (%)
1	0.12	0.69	1.29	0.25	1.85
2	0.06	0.277	0.106	0.24	0.117
3	0.08	0.410	2.58E-2	0.25	3.31E-2
4	0.08	0.477	5.12E-2	0.22	6.72E-2
5	1	0.308	6.01E-3	0.23	4.26E-4

Table 5.5: PSCs with Improved Substrate Cleaning

PSC	Active Area (cm^2)	V_{OC} (V)	I_{SC} (mA)	FF	Efficiency (%)
1	0.01	0.308	0.601	0.23	4.26
2	0.01	0.274	0.635	0.24	4.18
3	0.01	0.236	0.588	0.24	3.33
4	0.01	0.400	0.348	0.19	2.64
5	0.12	0.69	1.22	0.26	1.82

CHAPTER VI

CONCLUSION AND FUTURE WORK

A low temperature flexible PSC with TiO_2 NPs as a mesoporous ETL was developed in high humidity (65% – 70%) environment. A mesoporous TiO_2 ETL was deposited by spin coating which was composed of nanoparticles and annealed at low temperatures. A maximum efficiency of 4.82% has been achieved by the perovskite solar cell with an active area of $0.01cm^2$ and 1.84% for PSC with active area of $0.12cm^2$.

Future work consists of improving the efficiency of PSCs with bigger active area, smaller TiO_2 nanoparticles could be beneficial in order to create a thinner ETL in order for the PSC to have less resistance allowing for an improvement in the fill factor. Fabricating a ball mill for the milling of the TiO_2 nanofibers is also necessary in order to reduce the length of the nanofibers which will allow for better control of the layer's thickness. A solution with TiO_2 nanoparticles and nanofibers would be tested first and compared with PSCs that were fabricated using only TiO_2 nanoparticles and nanofibers in order to see the effects of only using TiO_2 nanofibers in PSC fabrication. Annealing temperature and time also needs to be further studied in order to analyze how it affects the perovskite formation. By annealing at a lower temperature for longer time with long cooling periods, an increase in perovskite grain could be obtained. Bigger grain sizes allow the PSCs to

generate higher efficiency due to the grains pushing against each other preventing pinhole formation.

Fabricating the PSCs in a glove box in order to control humidity levels and temperature is important in order to compare PSCs that were fabricated in a controlled environment over those fabricated in a high humidity environment with temperature that are not constant. Comparing 1-step and 2-step deposition of the perovskite needs to be compared in humid environments to determine which method produces better efficiency. Further study of the sputtering deposition of Ag for the back electrode needs to done in order to optimize the time needed to create an optimal layer thickness. Using a magnetron sputtering machine could also be beneficial in order to see if a higher PSC efficiency can be obtained with that deposition technique. In order to improve the layer morphology of the PSC, a chuck needs to be designed for the spin coating machine that does not create strain on the flexible substrates by reducing the area in which the vacuum pulls on the substrate.

REFERENCES

Aldibaja, F. K., Badia, L, Mas-Marza, E., Sanchez, R. S., Barea, E. M., Mora-Sero, I., "Effect of different lead precursors on perovskite solar cell performance and stability," *J. Mater. Chem. A*,pp. 9194-9200, 2015

Ball, J. M., Lee, M. M., Hey, A., and Snaith, H. J., "Low-temperature processed meso-superstructured to thin-film perovskite solar cells," *Energy Environ. Sci*., vol. 6, pp. 1739–1743, 2013

Berson, S., De Bettignies, R., Bailly, S., and Guillerez, S., "Poly(3-hexylthiophene) Fibers for Photovoltaic Applications," *Adv. Func. Mat.*, vol. 17, issue 8, pp. 1377-1384, 2007

Bertho, S., Oosterbaan, W. D., Vrindts, V., D'Haen, J., Cleij, T. J., Lutsen, L., Manca, J., and Vanderzande, D., "Controlling the morphology of nanofiber-P3HT:PCBM blends for organic bulk heterojunction solar cells," *Org. Electron.*, vol. 10, no. 7, pp. 1248–1251, 2009

Bi, D., Moon, S. J., Haggman, L., Boschloo, G., Yang, L., Johansson, E. M. J., Nazeeruddin, M. K., Gratzel, M., and Hagfeldt, A., "Using a two-step deposition technique to prepare perovskite ($CH_3NH_3PbI_3$) for thin film solar cells based on ZrO_2 and TiO_2 mesostructures," *RSC Adv.*, issue 41, 2013

Cao, K., Zuo, Z., Cui, J., Shen, Y., Moehl, T., Zakeeruddin, S. M., Grätzel, M., and Wang, M., "Efficient screen printed perovskite solar cells based on mesoscopic TiO_2/Al_2O_3/NiO/carbon architecture," *Nano Energy*, vol. 17, pp. 171–179, 2015

Casaluci, S., Cina, L., Pockett, A., Kubiak, P. S., Niemann, R. G., Reale, A., Di Carlo, A., and Cameron, P. J., "A simple approach for the fabrication of perovskite solar cells in air," *J. Power Sources,* vol. 297, pp. 504-510, 2015

Chen, Q. et al., "Planar heterojunction perovskite solar cells via vapor- assisted solution process," *J. Am. Chem. Soc*., vol. 136, pp. 622–625, 2014

Chen, Q., Zhou, H., Hong, Z., Luo, S., Duan, H. S., Wang, H. H., Liu, Y., Li, G., and Yang, Y., "Planar Heterojunction Perovskite Solar Cells via Vapor-Assisted Solution Process," *J. Am. Chem. Soc.*, 2013

Choi, H., Jeong, J., Kim, H. B., Kim, S., Walker, B., Kim, G. H., and Kim, J. Y., "Cesium-doped methylammonium lead iodide perovskite light absorber for hybrid solar cells," *Nano Energy*, vol. 7, pp. 80–85, 2014.

Chung, I., Lee, B., He, J., Chang, R. P. H., and Kanatzidis, M. G., "All-solid- state dye-sensitized solar cells with high efficiency," Nature, vol. 485, pp. 486–489, 2012

Deng, J., Liu, J., Wang, M., and Song, X., "The influence of blocking layer on the photovoltaic performance of organometal halide perovskite solar cell," *14th IEEE Int. Conf. Nanotechnol.*, pp. 789–793, 2014.

Di Carlo, A. and Matteocci, F., "Perovskite photovoltaics : from lab cells to modules," *15th International Converence on Environment and Electrical Engineering (EEEIC) IEEE* pp. 4–7, 2015.

Dong, X., Fang, X., Lv, M., Lin, B., Zhang, S., Ding, J., and Yuan, N., "Improvement of the humidity stability of organic-inorganic perovskite solar cells using ultrathin Al_2O_3 layers prepared by atomic layer deposition," *J. Mater. Chem. A,* 3 (10), pp. 5360-5367, 2015

Dkhissi, Y., Huang, F., Rubanov, S., Xiao, M., Bach, U., Spiccia, L., Caruso, R. A., and Cheng, Y. B., "Low temperature processing of flexible planar perovskite solar cells with efficiency over 10%," *J. Power Sources*, vol. 278, pp. 325–331, 2015

Dualeh, A., Gao, P., Seok, S. I., Nazeeruddin, M. K., Gratzel, M., "Thermal behavior of methylammonium lead-trihalide perovskite photovoltaic light harvesters," *Chem. Mater.* 26 (21), 6160–6164, 2014

Eperon, G. E., Burlakov, V. M., Docampo, P., Goriely, A., and Snaith, H. J., "Morphological control for high performance, solution-processed planar heterojunction perovskite solar cells," *Adv. Funct. Mater.*, vol. 24, pp. 151–157, 2014

Etgar, L. et al., "Mesoscopic CH3NH3 PbI3 /TiO2 heterojunction solar cells," *J. Am. Chem. Soc.*, vol. 134, pp. 17396–17399, 2012

Frost, J. M., Butler, K. T., Brivio, F., Hendon, C. H., Schilfgaarde, M. van, Walsh, A., "Atomistic origins of high-performance in hybrid halide perovskite solar cells," *Nano Lett.*, 14(5), pp. 2584-2590, 2014

Gratzel, M. "Dye Sensitized Solar Cells". Review.

Green, M. A."Solar cell fill factors: General graph and empirical expressions". *Solid-State Electronics*, vol. 24, pp. 788 – 789, 1981

Green, M., Ho-Baillie, A., Snaith, H., 2015. "The emergence of perovskite solar cells". *Nature Photonics 8,* 506-514

Guarnera, S., Abate, A., Zhang, W., Foster, J. M., Richardson, G., Petrozza, G., Snaith, H. J., "Improving the long-term stability of perovskite solar cells with a Porous Al_2O_3 buffer layer," *J. Phys. Chem. Lett*. 6 (3), pp. 432–437, 2015

Guo, Y., Liu, C., Inoue, K., Harano, K., Tanaka, H., and Nakamura, E., "Enhancement in the efficiency of an organic–inorganic hybrid solar cell with a doped P3HT hole-transporting layer on a void-free perovskite active layer," *J. Mater. Chem. A*, vol. 2, no. 34, pp. 13827–13830, 2014

Habisreutinger, S. N., Leijttens, T., Eperon, G. E., Stranks, S. D., Nicholas, R. J., and Snaith, H. J. "Carbon nanotube/polymer composites as a highly stable noble collection layer in perovskite solar cells," *Nano Lett.*, 14(10), pp. 5561-5568, 2014

Hanaor, D. A. H., Chironi, I., Karatchevtseva, I., Triani, G., and Sorrell, C. C. "Single and Mixed Phase TiO2 powders prepared by excess hydrolysis of titanium alkoxide". *Advances in Applied Ceramics*, 111 (3), 149 – 158, 2012

Heo, J. H., Im, S. H., Noh, J. H., Mandal, T. N., Lim, C. S., Chang, J. A., Lee, Y. H., Kim, H. J., Sarkar, A., Nazeeruddin, M. K., Gratzel, M. and Seok, S. I., "Efficient perovskite solar cells based on low-temperature solution-processed $(CH_3NH_3)PbI_3$ perovskite/$CulnS_2$ planar heterojunctions," *Nanoscale Res. Lett.*, vol. 9, 2014

Hodes, G., 2013. "Perovskite-Based Solar Cells". *Science Vol. 342 no. 6156* pp. 317-318

Hu, H., Wang, D,, Zhou, Y., Zhang, J., Lv, S., Pang, S., Chen, X., Liu, Z., Padture, N. P., and Cui, G., "Vapour-based processing of hole-conductor-free $CH_3NH_3PbI_3$ perovskite/C_{60} fullerene planar solar cells," *RSC Adv.* Issue 55, 2014

Hu, X., Du, P., Xu, W., Wang, K., Yi, C., Liu, C., Huang, F., Gong, X., and Cao, Y., "Efficient Perovskite Hybrid Solar Cells via Controllable Crystallization Film Morphology," vol. 5, no. 5, pp. 1402–1407, 2015

Huang, L., Hu, Z., Xu, J., Zhang, K., Zhang, J., and Zhu, Y., "Multi-step slow annealing perovskite films for high performance planar perovskite solar cells," *Sol. Energy Mater. Sol. Cells*, vol. 141, pp. 377–382, 2015

Jeng, J. Y. et al.,"CH3NH3 PbI3 perovskite/fullerene planar heterojunction hybrid solar cells," *Adv. Mater.*, vol. 25, pp. 3727–3732, 2013

Im, J., Lee, C., Lee, J., Park, S., and Park, N., "6.5% efficient perovskite quantum-dot-sensitized solar cell," *Nanoscale*, issue 10, 2011

Kazim, S., Nazeeruddin, M., Gratzel, M., and Ahmand, S., "Perovskite as light harvester: a game changer in photovoltaics," *Angew Chem. Int. Ed. Engl.*, 2014

Kim, H. S., Im, S. H., Park, N. G., "Organolead halide perovskite: New horizons in solar cell research," *J. Phys. Chem. C*, 118(11), pp. 5615-5625, 2014

Kojima, A., Teshima, K., Shira, Y., and Miyasaka, T., "Organometal Halide Perovskites as Visible-Light Sensitizers for Photovoltaic Cells," *J. Am. Chem. Soc.,* 131(17), pp. 6050-6051, 2009

Kim, J. H., William, S. T., Cho, N., Chueh, C. C., and Jen, A. K. Y., "Enhanced environmental stability of planar heterojunction perovskite solar cells based on blade-coating," *Adv. Energy Mater.,* 5(4), 2015

Lee, M., Teuscher, Miyasaka, J., Murakami, T., and Snaith, H., "Efficient Hybrid Solar Cells Based on Meso-Superstructured Organometal Halide Perovskites," *Science,* vol. 338, no. 6107, pp. 643-647, 2012

Lee, Y. H., Stefik, M., Heiniger, L., Gao, P., Seok, S. I. I., Grätzel, M., and Nazeeruddin, M. K., "Power from the Sun: Perovskite Solar Cells," *IEEE,* pp. 943–948, 2014

Leijtens, T., Eperon, G. E., Pathak, S., Abate, A., Lee, M. M., Snaith, H. J., "Overcoming ultraviolet light instability of sensitized TiO_2 with meso-superstructured organometal tri-halide perovskite solar cells," *Nat. Commun.* 4, 2885, 2013

Li, N., Zhu, R., and Yang, Y., "Polymer solar cells," *Nat Photon,* vol. 6, pp. 153-161

Liang, P. W. et al., "Additive enhanced crystallization of solution- processed perovskite for highly efficient planar-heterojunction solar cells," *Adv. Mater.,* vol. 26, pp. 3748–3754, 2014

Liang, Y. Y. et al., "For the bright future—Bulk heterojunction polymer solar cells with power conversion efficiency of 7.4%," *Adv. Mater.,*vol. 20, pp. E135–E138, 2010

Liu, D., and Kelly, T., "Perovskite solar cells with a planar heterojunction structure prepared using room-temperature solution processing techniques," *Nature Photonics,* vol 8, issue 2, pp. 133-138, 2014

Ma, Y., Zheng, L., Chung, Y. H., Chu, S., Xiao, L., Chen, Z., Want, S., Qu, B., Gong, Q., Wu, Z., and Hou, X., "A highly efficient mesoscopic solar cell based on $CH_3NH_3PbI_{3-x}Cl_x$ fabricated via sequential deposition," *Chem. Commun.,* issue 83, 2014

Mali, S. S., Kim, H. J., Shim, C. S., Patil, P. S., Kim, J. H., Hong, C. K., "Surfactant free most probable TiO2 nanostructures via hydrothermal and its dye sensitized solar cell properties", *Science,* Rep. 3, 2013

Mali, S. S., Shim, C. S., Kim, H., Patil, J. V., Ahn, D. H., Patil, P. S., and Hong, C. K., "Evaluation of various diameters of titanium oxide nanofibers for efficient dye sensitized solar cells synthesized by electrospinning technique: A systematic study and their application," *Electrochim. Acta,* vol. 166, pp. 356–366, 2015

Malinkiewicz, O. et al., "Perovskite solar cells employing organic charge- transport layers," Nature Photon., vol. 8, pp. 128–132, 2014

Mei, A., Li X., Liu, L., Ku, Z., Liu, T., Rong, Y., Xu, M., Hu, M., Chen, J., Yang, Y., Gratzel, M., and Han, H, "A hole-conductor-free, fully printable mesoscopic perovskite solar cell with high stability," *Science*, pp. 295-298, 2014

Miller, D., Yablonovitch, E., Kurthz, S., "Strong Internal and External Luminescence as Solar Cells Approach the Shockley-Queisser Limit," *Photovoltaics, IEEE Journal of*, vol. 2, issue 3, pp. 303-311, 2012

Nagarjuna, P., Narayanaswamy,K., Swetha, T., Rao, G. H., Singh, S. P., and Sharma, G. D., "CH3NH3PbI3 Perovskite Sensitized Solar Cells Using a D-A Copolymer as Hole Transport Material," *Electrochim. Acta*, vol. 151, pp. 21–26, 2015

Nair, S., Jose, R., Shengyuan, Y., and Ramakrishna, S., "A simple recipe for an efficient TiO2 nanofiber-based dye-sensitized solar cell," *J. Colloid Interface Sci.*, vol. 353, no. 1, pp. 39–45, 2011

Niu, G., Li, W., Meng, F., Wang, L., Dong, H., and Qiu, Y., "Study on the stability of $CH_3NH_3PbI_3$ films and the effect of post-modification by aluminum oxide in all-solid-state hybrid solar cells,"*J. Mater. Chem. A*, issue 3, 2013

Noh, J. H., Im, S. H., Heo, J. H., Mandal, T. N., Seok, S. I., "Chemical management for colorful, efficient, and stable inorganic-organic hybrid nanostructured solar cells," *Nano Lett.*, 13(4), pp. 1764-1769, 2013

Norman, K., Ghanbari-Siahkali, A., and Larsen, N. B., "6 Studies of spin-coated polymer films," *annu. Rep. Prog. Chem., Sect. C: Phys. Chem.*, vol. 101, 2005

O'regan, B., and Gratzel, M., "A low-cost, high-efficiency solar cell based on dye-sensitized colloidal TiO_2 films," *Nature*, 353, pp. 737-740, 1991

Park, G., "Perovskite solar cells: Switchable photovoltaics," *Nature*, vol 14, issue 2, pp. 140-141, 2015

Park, N. G., "Perovskite solar cells: an emerging photovoltaic technology," *Mater. Today*, vol. 18, no. 2, pp. 65–72, 2015

Ponseca Jr, C., Savenije, T., Abdellah, M., Zheng, K., Yartsev, A., Pascher, T., Harlang, T., Chabera, P., Pullerits, T., and Stepanov, A.,"Mechanism of Charge Transfer and Recombination Dynamics in Organo Metal halide Perovskites and Organic Electrodes, PCBM, and Spiro-OMeTAD: Role of Dark Carriers," *J. Am. Chem. Soc*. 137(51), pp. 16043-16048, 2015

Roiati, V., Colella, S., Lerario, G., De Marco, L., Rizzo, A., Listorti, A., and Gigli, G., "Investigating charge dynamics in halide perovskite-sensitized mesostructured solar cells," *Energy Environ. Sci.*, issue 6, pp. 1889-1894, 2014

Salam, Z., Vijayakumar, E., Subramania, A., Sivasankar, N., and Mallick, S., "Graphene quantum dots decorated electrospun TiO2 nanofibers as an effective photoanode for dye sensitized solar cells," *Sol. Energy Mater. Sol. Cells*, vol. 143, pp. 250–259, 2015

Shahbazi, M. and Wang, H., "Progress in research on the stability of organometal perovskite solar cells," *Solar Energy*, vol. 123. pp. 74–87, 2016

Shi, Y., Xing, Y., Li, Y., Dong, Q., Wang, K., Du, Y., Bai, X., Wang, S., Chen, Z., and Ma, T., 2015. "$CH_3NH_3PbI_3$ and $CH_3NH_3PbI_{3-x}Cl_x$ in Planar or Mesoporous Perovskite Solar Cells: Comprehensive Insight into the Dependence of Performance on Architecture." *J. Phys. Chem. C., 119(28)*, pp. 15868-15873

Stoumpos, C., Malliakas, C., and Kanatzidis, G., "Semiconducting Tin and Lead Iodide Perovskites with Organic Cations: Phase Transitions, High Mobilities, and Near-Infrared Photoluminescent Properties," *Inorganic Chemistry*, 52(15), pp. 9019-9038, 2013

U.S. Energy Information Administration (2016, Oct. 18). "How much electricity does an American home use?". Retrieved from https://www.eia.gov/tools/faqs/faq.cfm?id=97&t=3

U.S. Energy Information Administration (2015, Nov. 4). "Energy from the sun". Retrieved from www.eia.gov.

Wang, J. T. W., Ball, J. M., Barea, E. M., A. Abate, J. a. Alexander-Webber, J. Huang, M. Saliba, I. Mora-Sero, J. Bisquert, H. J. Snaith, and R. J. Nicholas, "Low-temperature processed electron collection layers of graphene/TiO_2 nanocomposites in thin film perovskite solar cells," *Nano Lett.*, vol. 14, no. 2, pp. 724–730, 2014

Wang, K., Liu, C., Du, P., Chen, L., Zhu, J., Karim, A., and Gong, X., "Efficiencies of perovskite hybrid solar cells influenced by film thickness and morphology of CH3NH3PbI3−xClx layer," *Org. Electron.*, vol. 21, pp. 19–26, 2015

Wang, X., Li, X., Tang, G., Zhao, L., Zhang, W., and Jiu, T., "Improving efficiency of planar hybrid $CH_3NH_3PbI_3$-xClx perovskite solar cells by isopropanol solvent treatment," *Org. Electron.*, vol. 24, no. May, pp. 1–7, 2015

Wu, R., Yang, J., Xiong, J., Liu, P., Zhou, C., Huang, H., Gao, Y., and Yang, B., "Efficient electron-blocking layer-free planar heterojunction perovskite solar cells with a high open-circuit voltage," *Org. Electron.*, vol. 26, pp. 265–272, 2015

Wu, Y., Islam, A., Yang, X., Qin, C., Liu, J., Zhang, K., Peng, W., and Han, L., "Retarding the crystallization of PbI_2 for highly reproducible planar-structured perovskite solar cells via sequential deposition," *Energy Environ. Sci.*, issue 9, 2014

Xiao, J., Shi, J., Liu, H., Xu, Y., Lv, S., Luo, Y., Li, D., Meng, Q., Li, Y., "Efficient $CH_3NH_3PbI_3$ perovskite solar cells based on graphydine (GD)-modified P3HT hole-transporting material," *Adv. Energy Mater.,* 2015

Xing, G. C. et al., "Long-range balanced electron- and hole-transport lengths in organic-inorganic $CH_3NH_3PbI_3$," *Science,* vol. 342, pp. 344– 347, 2013

Yang, D., Yang, Z., Qin, W., Zhang, Y., Liu, S., and Liu, C., "Alternating precursor layer deposition for highly stable perovskite films towards efficient solar cells using vacuum deposition," *J. Mater. Chem. A,* 3(18), pp. 9401-9405, 2015

Yang, Z., Cai, B., Zhou, B., Yao, T., Yu, W., Liu, S. (Frank), Zhang, W. H., and Li, C., "An up-scalable approach to CH3NH3PbI3 compact films for high-performance perovskite solar cells," *Nano Energy,* vol. 15, pp. 670–678, 2015

You, J., Hong, Z., Yang, Y., and Zhou, H., "Low temperature solution-processed perovskite solar cells with high efficiency an flexibility.", *ACS Nano 8(2),* 2014

Zeman, M. "Introduction to Photovoltaic Solar Energy". pp. 4.1 – 5.12

Zhang, W., Anaya, M., Lozano, G., Calvo, M. E., Johnston, M. B., Miguez, H., and Snaith, H. J., "Highly Efficient Perovskite Solar Cells with Tunable Structural Color," *Nano Lett.,* issue 15, pp. 1698-1702, 2015

Zhang, Y., Yu, W., Qin, W., Yang, Z., Yang, D., Xing, Y., Liu, S. (Frank), and Li, C., "Perovskite as an effective Voc switcher for high efficiency polymer solar cells," *Nano Energy,* pp. 1–8, 2015

Zhou, H., Chen, Q., Li, G., Luo, S., Song, T. B., Duan, H. S., Hong, Z., You, J., Liu, Y., and Yang, Y., "Interface engineering of highly efficient perovskite solar cells," *Science,* vol. 345, no. 6196, pp. 542-546, 2014

Zhou, H. P. et al., "Interface engineering of highly efficient perovskite solar cells," *Science,* vol. 345, pp. 542–546, 2014

APPENDIX

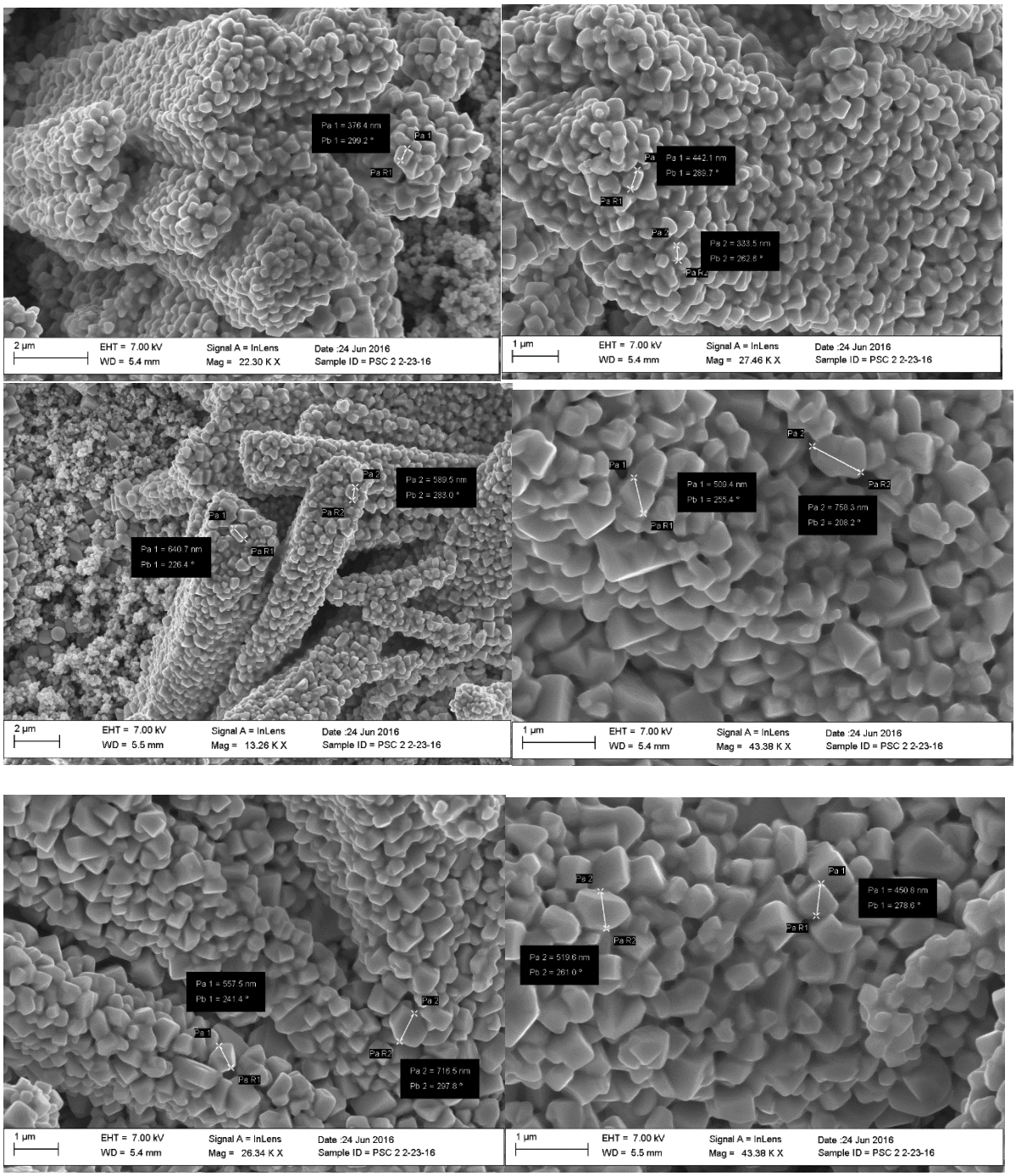

Figure A.1: Perovskite Grain Sizes

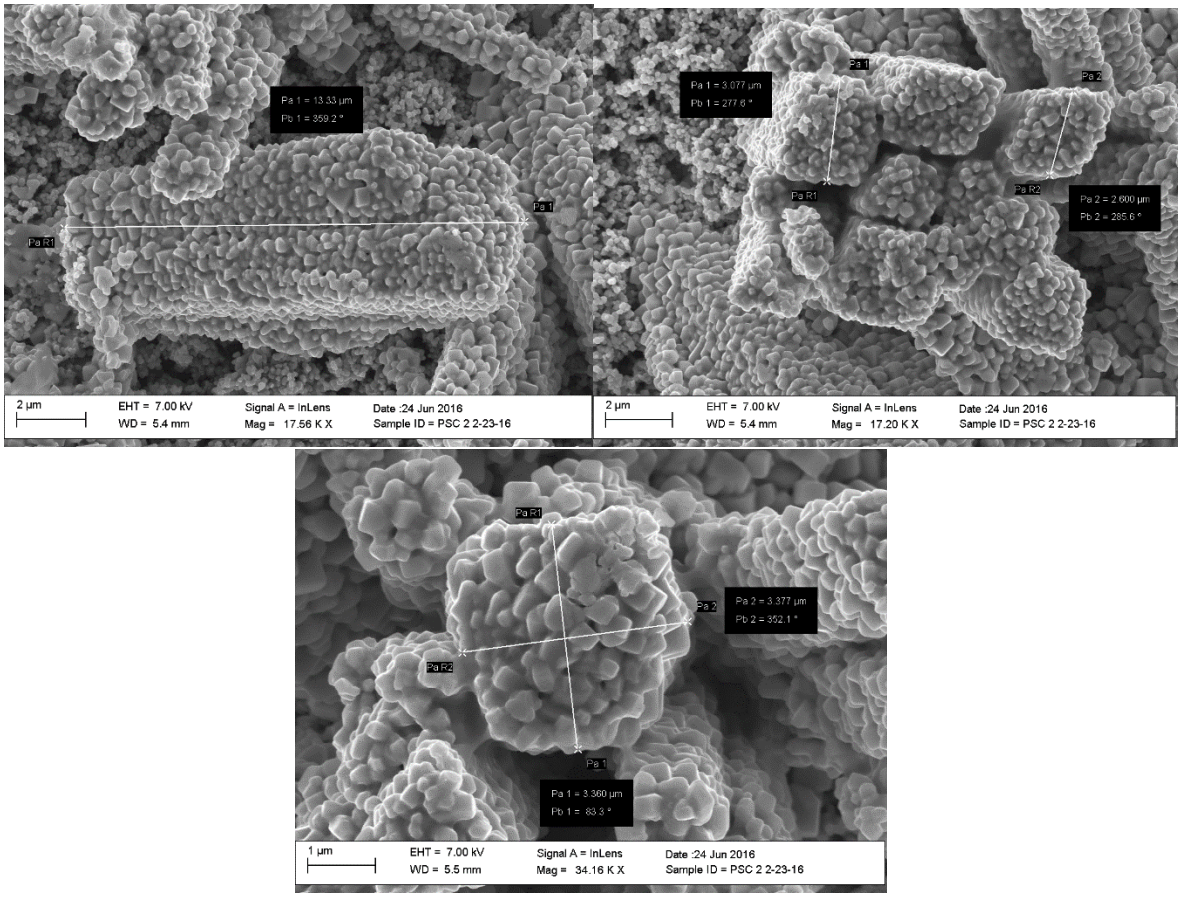

Figure A.2: Perovskite Rods

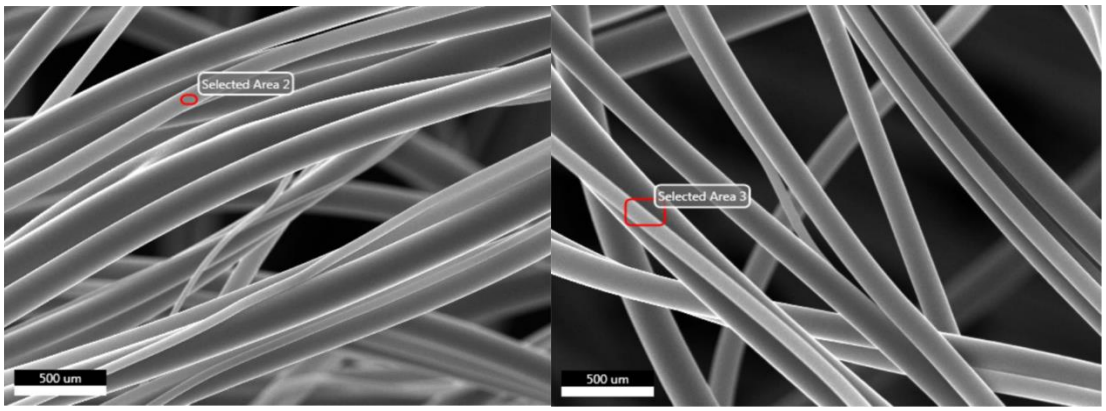

Figure A.3: TiO_2 NF with Acetic and Glacial Acetic Acid

ABBREVIATIONS

Characterization

A_C – area of collector

EDAX – energy dispersive x-ray spectroscopy

FESEM – field emission scanning electron microscope

F – incident radiation flux

FF – fill factor

J_0 – dark saturation current density

J(V) – net current density

J_L – light generated current density

J_{mp} – maximum power current density

J_{SC} – short circuit current density

K – Boltzmann's constant

m – ideal factor in diode equation

PCE or η – power conversion efficiency

P_{in} – input power

P_{max} – peak power

q – elemental electron charge

T – absolute temperature

V_{mp} – maximum power voltage

V_{OC} – open circuit voltage

Materials

Ag – silver

CH_3NH_3I – methylammonium iodide

$CH_3NH_3PbI_3$ – methylammonium lead iodide

DMF – Dimethylformamide

MAI – methylammonium iodide

MAPI or MAPI – methylammonium lead iodide

NF – nanofiber

NP – nanoparticle

P3HT – poly(3-hexylthiophene-2,5-diyl)

PCBM – Phenyl-C60-butyric acid methyl ester

PEDOT:PSS – Poly(3,4-ethylenedioxythiophene)-poly(styrenesulfonate)

TiO_2 – titanium dioxide

TTIP – titanium (IV) isopropoxide

Solar Cell Fabrication

BC – blade coating

DC – dip coating

DSSC – dye sensitized solar cell

ETL – electron transport layer

ETM – electron transport material

FTO – fluorine doped tin oxide

HTL – hole transport layer

HTM – hole transport material

ITO – indium tin oxide

PET – polyethylene terephthalate

PSC – perovskite solar cell

SC – spin coating

SpC – spray coating

BIOGRAPHICAL SKETCH

Felipe De La Torre graduated on December 2013 with his bachelors in Electrical Engineering at The University of Texas Pan American where he continued his studies and got accepted into the graduate program. He started working as a Research Assistant under Dr. Wenjie Dong in the area of nonholonomic mobile robots for a year were he had to program mobile robots to move in a formation. After the funding for the project ended in 2015, he went to work as a Research Assistant under Dr. Karen Lozano in the area of nanotechnology. Here he assisted in the development of a prototype of a compact and portable handheld device capable of generating nanofibers composed of different polymers and started his research in perovskite solar cells. He obtained his master's degree on December 2016 at The University of Texas Rio Grande Valley.

E-mail address: felipedlatorre@gmail.com